Chapter-3

A Molecular Theory for Phase Diagrams Involving Smectic and Nematic Phases Exhibited by Strongly Polar Compounds.

3.1 Introduction

As described in chapter-1 (see section 1.2), in the uniaxial nematic (N) liquid crystal composed of rod like molecules, the long axes of the rods tend to be aligned along the *director* represented by the unit vector $\hat{\boldsymbol{n}}$ (see figure 1.1, chapter-1). The extent of orientational order is represented by the order parameter S defined as

$$S = \tfrac{1}{2}\langle 3\cos^2\theta_i - 1\rangle = \langle P_2(\cos\theta_i)\rangle \tag{3.1}$$

where θ_i is the angle between the long axis of the i^{th} molecule and the director, P_2 is the second Legendre polynomial and $\langle\ \rangle$ denote a statistical average.

In smectic liquid crystals, the centres of mass of the rods have an additional quasi long range one dimensional periodic order. The resulting density modulation, on Fourier analysis, can be expressed in a series of sinusoidal functions. Of these, the dominant one is the first harmonic. Hence, the smectic density wave can be represented by

$$\rho(z) = \rho_o[1+\tau\cos(qz)] \tag{3.2}$$

where ρ_o is the average density of the medium, $\vec{\boldsymbol{q}}$ is the wave vector along the layer normal with $q = |\vec{\boldsymbol{q}}| = 2\pi/d$ and d is the average spacing of the layers. We choose the laboratory frame of reference with the Z-axis along the layer normal. The extent of layering (smectic) order is measured by the normalised amplitude of this density wave, called the smectic order parameter τ, given by

$$\tau = \langle\cos(2\pi z_i/d)\rangle \tag{3.3}$$

where, z_i is the z coordinate of the centre of mass of the i^{th} molecule. When there is no layering order, $\tau = 0$ and the medium has uniform density ρ_o corresponding to the

nematic or the isotropic phase. Different variations of layering and inlayer order are possible leading to different types of smectic liquid crystals. If $\vec{q}\tau\hat{n}$, *i.e.*, the director is normal to the layers, it is termed as the smectic A (SmA) liquid crystal (see figure 1.2, chapter-1). In this chapter, we describe various phase transitions involving SmA and nematic liquid crystals in highly polar compounds. We begin with a review of the experimental results.

3.1.1 The SmA-N transition

As explained in chapter-1 (see section 1.4), on cooling mesogenic compounds from the isotropic (I) phase, before transforming into a solid crystal (K), the shorter homologues exhibit the nematic (N) phase while the longer homologues exhibit the smectic A phase also. *i.e.*, the usual sequences of phase transitions are: I $\wedge$ N $\wedge$ K or I $\wedge$ N $\wedge$ SmA $\wedge$ K or I $\wedge$ SmA $\wedge$ K. Often, the shorter homologues of the smectogens exhibit a second order SmA-N transition at which the order parameter τ continuously goes to zero. As the chain length is increased, the nature of the transition changes over to first order and also the temperature range of the N phase decreases and finally vanishes. Very long homologues exhibit a first order SmA-I transition. A typical phase diagram illustrating the vanishing of the N phase for higher homologues is shown in

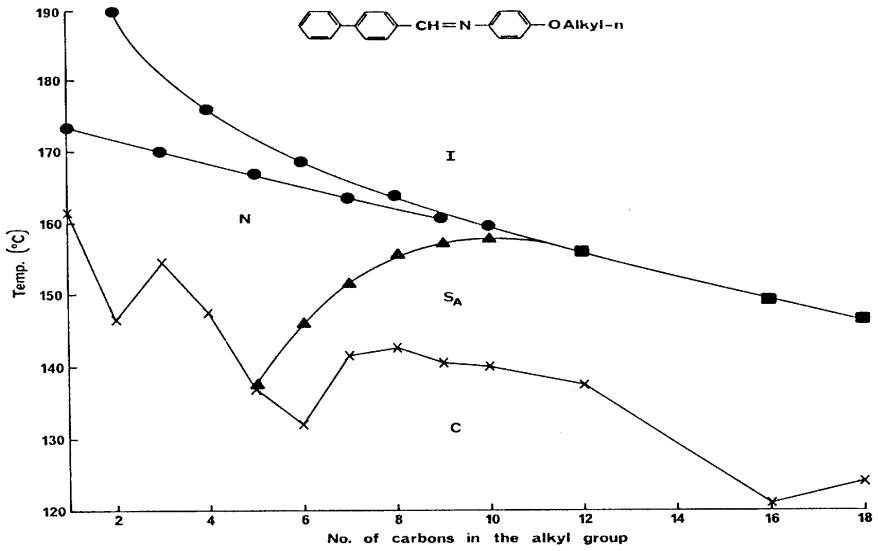

figure 3.1.

Figure - 3.1. Plot of liquid crystal transition temperatures against the number of carbon atoms (*n*) in the chain for *n*-alkoxy benzylidene amino biphenyls [1]. λ, σ, ν and 5represent N-I, SmA-N, SmA-I and C-N or C-

SmA transition respectively, where C denotes the solid crystal. The two branches in the N-I transition curve correspond to the odd (lower branch) and even (upper branch) values of *n*.

Liquid crystals made of ***strongly polar*** molecules exhibit some unusual phase sequences. We describe these in the next few sections.

3.1.2 Nematic reentrance

The structural formula of the strongly polar compound *n*-alk**o**xy **c**yano **b**iphenyl (*n*OCB), where *n* stands for the number of carbon atoms in the alkoxy chain, is shown below.

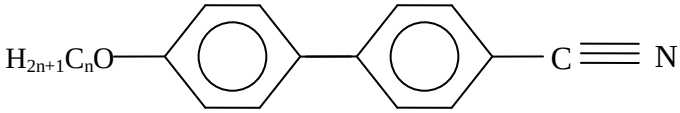

The sequence of phase transitions is I (78) N (56) K for 6OCB and I (79.5) N (67) SmA (54) K for 8OCB, where the numbers in the parenthesis represent the transition temperatures in ^{0}C.

Cladis [2] found that mixtures of certain compounds with strongly polar cyano or nitro end groups, on cooling from the isotropic phase, exhibit the sequence of transitions: I$\wedge$ N $\wedge$ SmA $\wedge$ N_R $\wedge$ K. The second nematic phase that occurs at temperatures lower than the range of occurrence of smectic phase is called the *re-entrant* nematic (N_R) phase (*eg*, 6OCB and 8OCB mixture, figure 3.2a). A similar phenomenon was found later on in pure compounds under elevated pressures (*eg.*,8OCB) [3] (figure 3.2b). Subsequently such a phase sequence has been found in some pure compounds at normal pressures also, for *eg.*, in Octyl**o**xy**b**enzyloxy-**b**enzylidene-**c**yanoaniline (OBBC) [4].

3.1.3 Double reentrance

On cooling further, below the N_R phase, another smectic phase re-enters in some pure compounds or binary mixtures leading to the sequence: I $\wedge$ N $\wedge$ SmA_d $\wedge$ N_R $\wedge$ SmA_1 $\wedge$ K. This phenomenon is called *double re-entrance*. The lower temperature re-entrant smectic phase, called the smectic-A_1 (SmA_1) phase, is found to have a layer spacing $d \approx l$, whereas the higher temperature smectic phase, called the smectic-A_d (SmA_d) phase, has $l < d < 2l$, where l is the molecular length. This partial bilayer

arrangement is understood on the basis of formation of appropriate antiparallel dimers of the molecules and hence the suffix ‘d’ is used to denote *dimers* and the suffix ‘1’ for the *monomers* (see section 1.6.5, chapter-1).

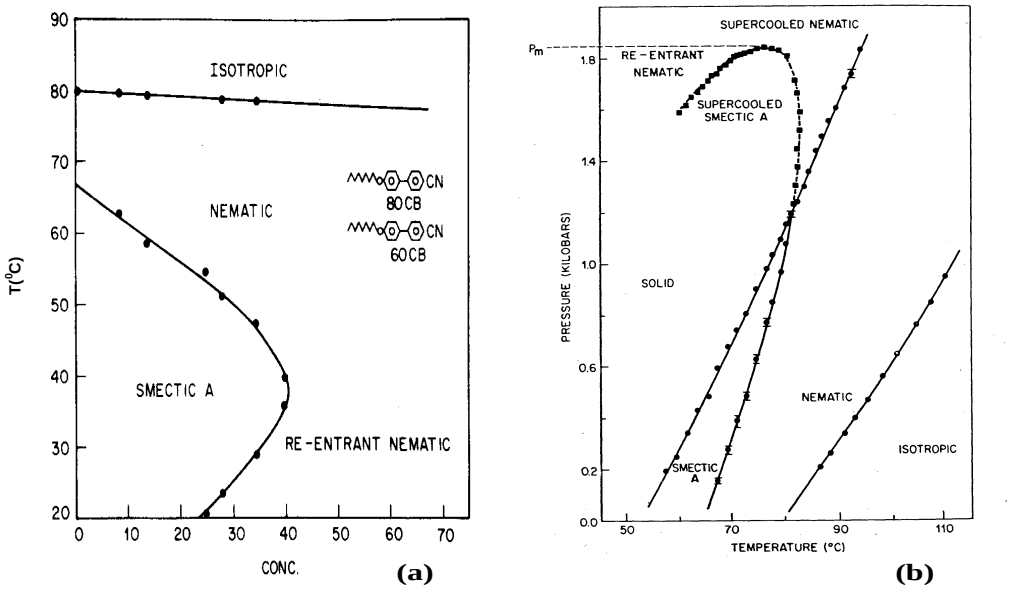

Figure - 3.2. (a) A typical temperature(*T*) - concentration (*X*) phase diagram of a binary mixture of polar compounds with *X* as wt% of 6OCB in 8OCB showing the nematic reentrance. The reentrant nematic occurs in the in the super cooled regime and the melting line is not shown [5]. (b) A reentrant phase sequence in pressure (*p*) - temperature (*T*) phase diagram for 8OCB [3].

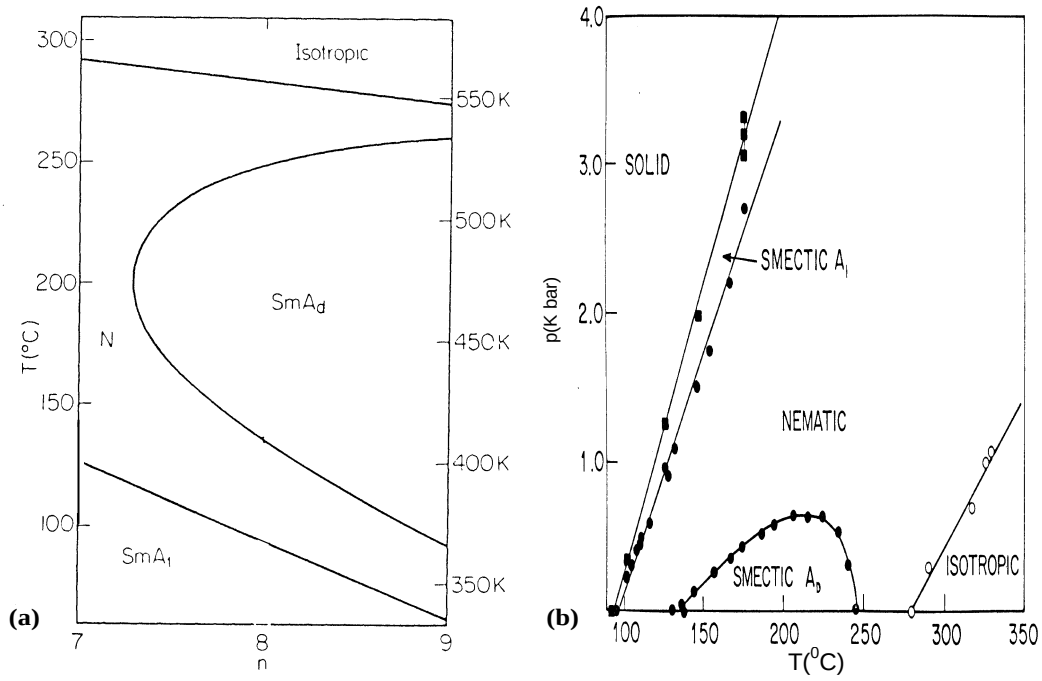

Figure - 3.3. (a) The temperature (*T*) - concentration phase diagram for binary mixtures of *n*-alkyloxybenzoyloxycyano-stilbene (*n* shown along the X- axis) showing the double reentrance with the bounded SmA_d phase [6]. (b) The pressure (*p*) - temperature (*T*) phase diagram [7] of the homologue with *n* = 8 showing similar features.

For example the compound octyloxybenzoyloxy cyano- stilbene (T8) shows double reentrance [8]:

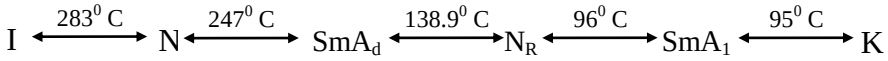

When the relative concentration in case of a binary mixture or the pressure applied to a pure compound is varied, the SmA_d phase gets bounded. This is shown in figure 3.3

3.1.4 Multiple reentrance and reentrant nematic lake

A few pure compounds, show a *quadruple re-entrant* sequence *viz.* $I\wedge N\wedge SmA_d \wedge N_R\wedge SmA_{dR}\wedge N_R\wedge SmA_1$ as the temperature is lowered. Multiple reentrance in the pure compound DB_9ONO_2 (the ninth homologue of *n*-alkoxyphenyl-nitrobenzoyloxybenzoate, DB_nONO_2) at atmospheric pressure was first reported by Tinh *et al* [9] though they did not identify all the phases. Later, DB_9ONO_2 was found to show the sequence [10],

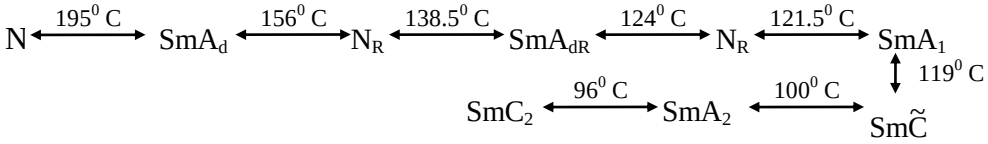

In the above, it may be noted that, apart from the SmA phases, the compound also exhibits the $Sm\tilde{C}$ phase which has, in the layers with tilted arrangement of molecules, the aromatic and the aliphatic parts alternating with some periodicity. The SmA_2 phase has $d\approx 2l$ and SmC_2 is the tilted version of SmA_2. In our theoretical models we do not consider the $Sm\tilde{C}$, SmA_2 and the SmC_2 phases. The 10^{th} homologue ($DB_{10}ONO_2$) exhibits a similar sequence at higher pressures (see figure 3.4a) [11]. This behaviour is also seen in some mixtures over a very narrow range of concentrations (*eg.,* ~50% molar mixture of DB_8ONO_2 and $DB_{10}ONO_2$) [10] (see

figure 3.4b). The temperature - concentration phase diagrams of mixtures of polar compounds not belonging to the same homologous series show other interesting features like a re-entrant nematic lake surrounded by the SmA phase [12] or a SmA_d island surrounded by the nematic region [13] (figure 3.4- c, d). A detailed review of various experimental studies on the SmA_d-SmA_1 phase transition boundary and the N_R region has been given by Shashidhar *et al* [14]. We do not specifically discuss SmA_d-SmA_2 critical point on the basis of our theory. Experimentally this transition has been studied in detail by Shashidhar *et al* [15].

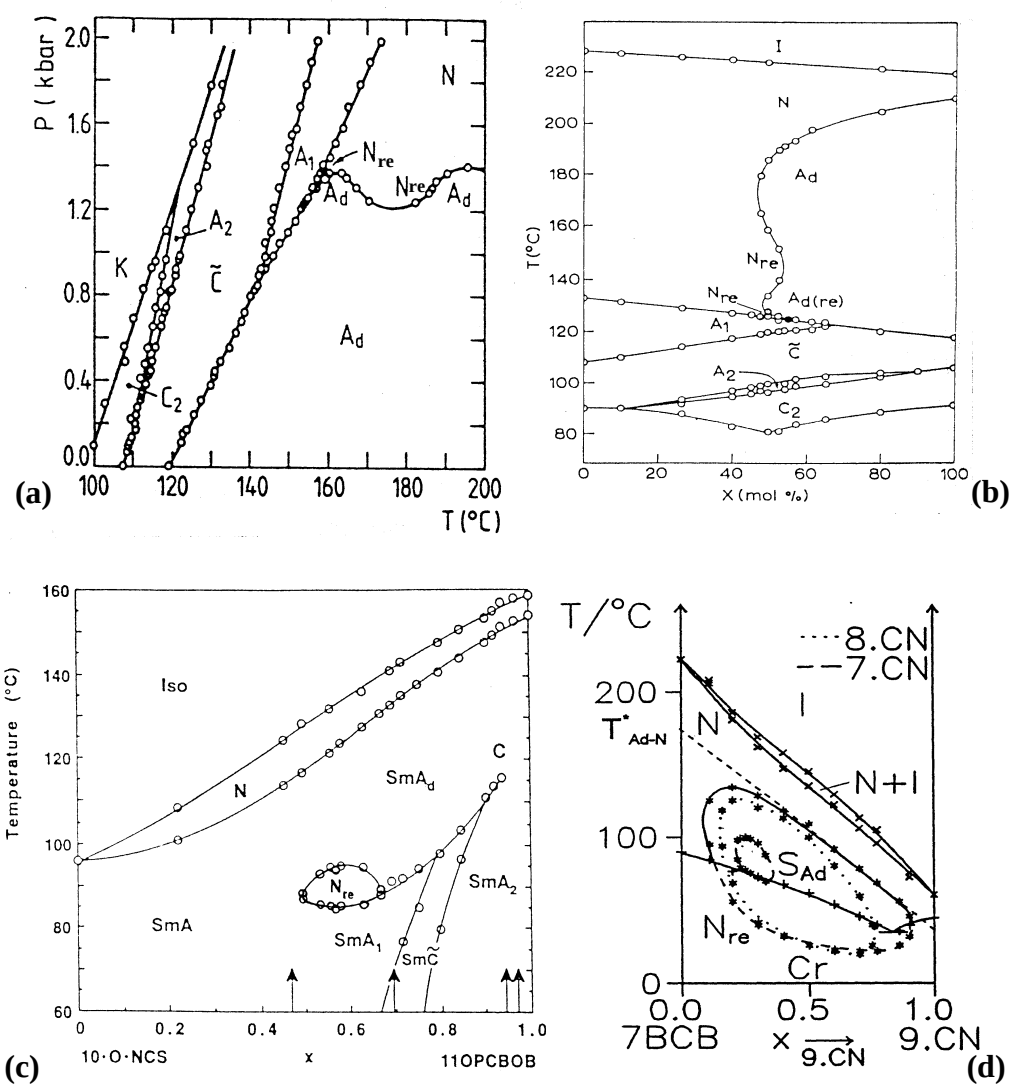

Figure-3.4.(a)The pressure-temperature phase diagram showing multiple reentrance and different smectic phases in $DB_{10}ONO_2$ [11]. (b) Similar phenomenon in temperature – concentration (*X*) plane in binary mixtures,

with *X* as the mole % of $DB_{10}ONO_2$ in DB_8ONO_2 [10]. In (a) and (b), SmA_1, SmA_d and SmA_2 are denoted as A_1, A_2 and A_d respectively. (c)Re-entrant nematic lake surrounded by the SmA phase [12] where, 10.O.NCS is decyloxy isothiocyanatophenyl benzoate and 11OPCBOB is undecyloxyphenyl cyanobenzyloxy benzoate. (d) SmA_d (denoted as S_{Ad}) island surrounded by the nematic region where *n*BCB is cyano biphenylyl *n*-alkylbenzoate and *n*CN is cyanophenyl *n*-alkyl benzoate [13]. In all the diagrams, the reentrant nematic is denoted as N_{re}.

There have been many attempts to explain double reentrance using phenomenological as well as molecular theories. Prost has developed a very successful Landau theory of the various phases exhibited by such compounds [16]. We have given a brief review of this theory in chapter-1 (see section 1.6.4). In the next section, we give some of the phase diagrams predicted by an extension of this theory by Prost and Toner [17].

3.1.5 Phase diagrams predicted by Prost's phenomenological theory

Different types of phase diagrams have been predicted by the phenomenological theory developed by Prost [16, 17] depending on the parameters used. In the theory, two coupled smectic order parameters corresponding to the molecular length l and another incommensurate length l' such that $l < l' < 2l$, have been used. Some of the phase diagrams predicted by this model are shown in the figures 3.5 and 3.6.

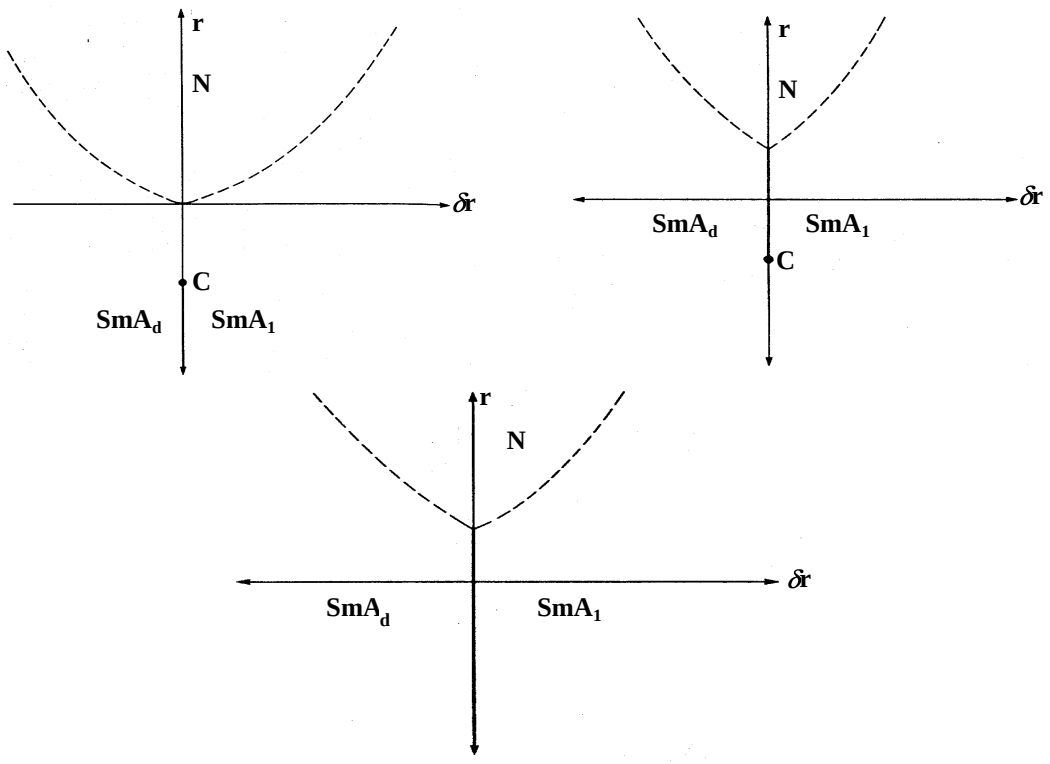

Figure- 3.5. Phase diagrams involving SmA_1, SmA_d and N phases, predicted by the dislocation loop melting theory of Prost and Toner [17] without considering fluctuations. The thick and the dashed lines indicate first and the second order phase transitions respectively and C denotes a critical point. r and δr are general variables which can be mapped to pressure and temperature or pressure and concentration *etc*.

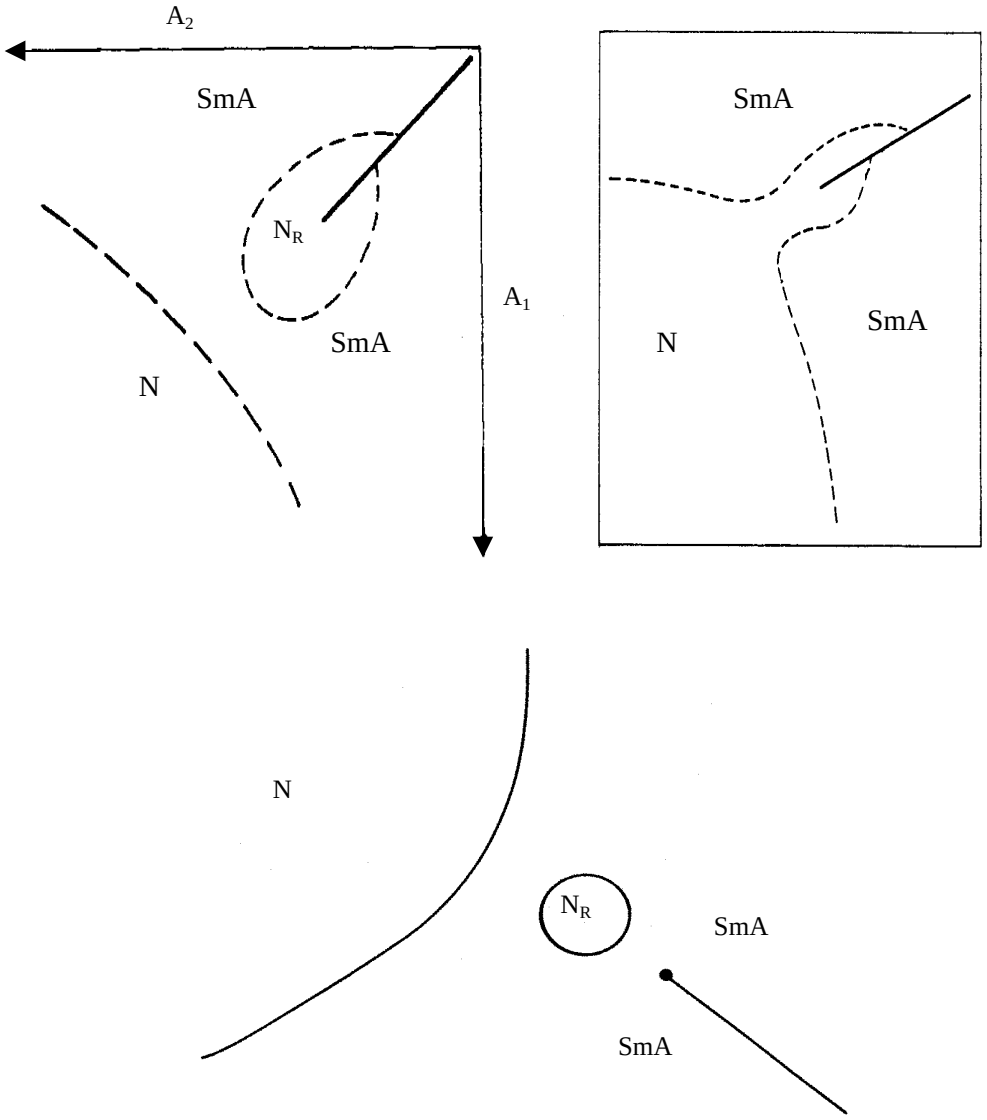

Figure-3.6. Phase diagrams predicted by the fluctuation-corrected dislocation loop melting theory of Prost and Toner [17]. A_1 and A_2 are general variables which can be mapped to pressure and temperature or pressure and concentration *etc*.

As de Gennes and Prost remark [16], "if the phenomenological approach provides a unifying framework for the description of the frustrated smectics, it does not give much detail on what is happening at a molecular scale". In the next section we discuss the molecular origin of the 'two lengths' assumed by Prost.

3.1.6 Molecular origin of the 'two lengths' assumed in Prost's model

Various theories have been proposed to explain the molecular origin of the 'two lengths' assumed by Prost. In all the molecular theories, the SmA_d structure is explained by assuming that the medium consists of antiparallel dimers [18] having the overlap of the aromatic parts. In the compounds which show double reentrance, the lower temperature smectic liquid crystals (SmA_1) has the *monolayer* structure [19]. We have reviewed several molecular models which have been proposed for the strongly polar compounds in section 1.6.5, chapter-1. We have also described in chapter-2, a simple model proposed by Madhusudana and Jyothsna Rajan [20], to explain the molecular origin of the 'two lengths' assumed in the Prost's phenomenological model [16]. The basic idea in this model is that the molecular pairs can change over from the anti-parallel (A) to the parallel (P) configuration as the intermolecular separation (r) is reduced due to cooling or due to increase of pressure. This change over occurs due to a competition between the repulsive dipole-dipole interaction and the attractive dipole-induced dipole and chain-chain interactions (see section 2.2, chapter-2). Recent experiments [21] showing the presence of *polar* short range order at low temperatures support this model. The model [20], with suitable modifications, gives a variety of phase diagrams. In chapter-2, we adopted this model for describing the N_1-N_d transition. In this chapter, we extend this model and develop a molecular theory of smectic mixtures, on the basis of the McMillan [22] theory of SmA liquid crystals. In the next section we give a brief review of the McMillan theory.

3.2 The McMillan theory of SmA liquid crystals

McMillan extended the Maier and Saupe (MS) [23] theory by including a potential corresponding to the one dimensional translational order of SmA liquid crystals. As explained in chapter-1 (see section 1.4.2), the compounds exhibiting the SmA phase usually have a central aromatic core and flexible alkyl chains at the two ends. The dispersion interaction energy is very strong between the aromatic moieties since they have large polarisabilities. Thus the aromatic parts of the neighbours tend to overlap and arrange themselves in a layer. The layer-structure is stabilised if the alkyl chains, which separate the layers, are sufficiently long. This is the physical idea

behind the model proposed by McMillan. Starting from an anisotropic pair interaction energy, and restricting the expansion to only one Fourier component, McMillan wrote the single particle potential of the i^{th} molecule as

$$U_i(\cos\theta_i, z_i) = -U_o\,[1+ \alpha\,\sigma\cos(2\pi z_i/d)]\,S\,(3\cos^2\theta_i - 1)/2 \qquad (3.4)$$

where U_0 is the MS interaction parameter, θ_i the angle between the long axis of the i^{th} molecule and the director, S the orientational order parameter defined in equation 3.1 above, d the layer spacing, z_i the coordinate of the centre of the i^{th} molecule measured along the layer normal and σ the coupled order parameter, which is a measure of the amplitude of the density wave in the SmA phase, defined by

$$\sigma = \langle\cos(2\pi z_i/d)\,(3\cos^2\theta_i - 1)/2\rangle. \qquad (3.5)$$

in which $\langle\rangle$ denote a statistical average. The McMillan parameter α is given by

$$\alpha = 2\exp[-(\pi r_o/d)^2] \qquad (3.6)$$

where r_0 which represents the 'range' of the dispersion interaction is of the order of the length of the rigid core of the molecules.

The molar internal energy is given by

$$U = \frac{N}{2}\langle U_i\rangle = -\frac{N}{2}U_0(S^2 + \alpha\sigma^2) \qquad (3.7)$$

where N is the Avogadro number. The factor (1/2) arises since each molecule is counted twice while finding the average. The molar entropy is written as

$$\mathcal{S} = -Nk_B\langle\ln f(z,\cos\theta)\rangle \qquad (3.8)$$

where k_B is the Boltzmann constant and $f(z,\cos\theta)$ is the normalised single particle distribution function. The molar Helmholtz free energy is written as

$$F = U - T\mathcal{S}. \qquad (3.9)$$

The normalised distribution function found by minimising the free energy is given by

$$f(z_i,\cos\theta_i) = Z^{-1}\exp(-U_i/k_BT) \qquad (3.10)$$

where Z is the normalising integral. The order parameters S and σ are calculated using

$$S = \frac{1}{d}\int_{-d/2}^{+d/2} dz \int_{0}^{1} d(\cos\theta)\, f(\cos\theta) P_2(\cos\theta). \tag{3.11}$$

$$\sigma = \frac{1}{d}\int_{-d/2}^{+d/2} dz \int_{0}^{1} d(\cos\theta)\, f(\cos\theta) \cos(2\pi z/d)\, P_2(\cos\theta). \tag{3.12}$$

The above equations have the following solutions:

(i) $S = 0$, $\sigma = 0$ corresponding to the isotropic phase,

(ii) $S \neq 0$, $\sigma = 0$, corresponding to the nematic phase,

(iii) $S \neq 0$, $\sigma \neq 0$, corresponding to the SmA phase. (3.13)

The MS condition is given by

$$U_0/k_B T_{NI} = 4.541 \tag{3.14}$$

where T_{NI} is the N-I transition temperature. Hence, U_0 just fixes the N-I transition temperature. The McMillan parameter α is a measure of the strength of the layering potential. It is clear from equation 3.6 that, for a given core length r_0, the value of α increases with an increase of the layer spacing d, *i.e.*, α increases with the increase of chain length in a homologous series. Thus the temperature- α phase diagrams of the McMillan theory are compared with the temperature-chain length phase diagrams obtained in experiments.

McMillan showed that, $\alpha < 0.7$ results in a second order SmA-N transition, which becomes first ordered in nature for $\alpha \geq 0.7$, *i.e.,* the phase diagram has a tricritical point at $\alpha = 0.7$. Further, the SmA phase has a direct transition to the isotropic phase for $\alpha \geq 0.98$. The theoretical phase diagram broadly reflects the experimental trends (see figure 3.1) in a homologous series.

We now extend the McMillan theory to develop a theory for smectic liquid crystals made of strongly polar compounds. For simplicity, we first consider the nematic order to be saturated, *i.e.*, S=1.

3.3 Theory of smectic liquid crystals made of strongly polar compounds with a saturated nematic order

3.3.1 Theoretical model

3.3.1.1 Assumptions

In order to simplify the calculations, the following assumptions are made.

(1) As mentioned above, the nematic order is taken to be saturated and only the smectic interactions are considered.

(2) For the sake of simplicity, as explained in chapter-2, we assume that the medium consists of *pairs* of molecules which have either an antiparallel (A) or parallel (P) configuration.

(3) As we described in chapter-2, the A-type (P-type) configuration is favoured at lower (higher) densities (see section 2.2, Chapter-2). The energy difference between the two configurations is written as

$$\Delta E = E_A - E_P = R_1 k_B T^* \left(\frac{R_2}{T_R} - 1 \right) \tag{3.15}$$

where k_B is the Boltzmann constant, E_A and E_P are the configurational energies of the A-type and P-type pairs respectively, T^* is some reference temperature, $R_1 k_B T^*$ is an interaction parameter and $T_R = T/T^*$ is the reduced temperature. R_2 is the reduced temperature at which the density of the medium is such that ΔE becomes zero. For $T_R > R_2$, the A-type configuration has the lower energy.

(4) The McMillan parameters for A-type (α_A) and P-type (α_P) configurations can be written as

$$\alpha_A = 2 \exp(-[\pi r_o / (r_o + 2c)]^2) \tag{3.16}$$

and

$$\alpha_P = 2 \exp(-[\pi r_o / (r_o + c)]^2) \tag{3.17}$$

where r_o and c are the lengths of the aromatic and chain moieties of the molecule respectively. α_P can be expressed in terms of α_A using

$$\frac{c}{r_0} = \frac{1}{2}\left[\frac{\pi}{\sqrt{\ln(2/\alpha_A)}} - 1\right]. \tag{3.18}$$

(5) It is clear that the geometrical parameters of the A and P types of configurations are different. Hence, as in case of nematic potential used in chapter-2, we assume the mutual smectic interaction parameter

$$\alpha_{AP} = \alpha_{PA} = \alpha_E = Q\sqrt{\alpha_A\,\alpha_P} \tag{3.19}$$

where $Q \neq 1$ indicates a deviation from the geometric mean (GM) approximation for the mutual smectic interaction and $(Q-1)$ is a measure of this deviation.

(6) In the previous chapter, ΔE was taken to be a function of temperature only (see equation 3.15 above). But, we note that the nematic lake is found in mixtures of chemically dissimilar compounds. Hence, an exact description of this phenomenon requires a general theory of mixtures. However, for the sake of simplicity we assume that the McMillan parameter α_A (or α_P) is adequate to represent a given concentration in such mixtures. In a homologous series, the chain length of the molecule and hence α vary. The chain-chain interaction energy and hence E_P can also be expected to vary with α. We assume that

$$\Delta E \propto (\alpha_A)^n \tag{3.20}$$

As in chapter-2, the value of ΔE is calculated for r = 0.5 nm for various values of chain length c, with the core length equivalent to that of 10 carbon bonds, dipole moment p = 6 Debye = 2×10^{-29} Cm, polarisability of the core =20Å^3 = 20×10^{-30}m^3 and chain-chain interaction constant $\approx1.1\times10^{-77}$ SI units/carbon bond (see section 2.2, chapter-2 for details). α_A is calculated using equation 3.16 above. By plotting $\ln(\Delta E/10^{-19}\text{J})$ as a function of $\ln(\alpha_A)$, it is seen that the slope ≈ 4 for the range of α_A

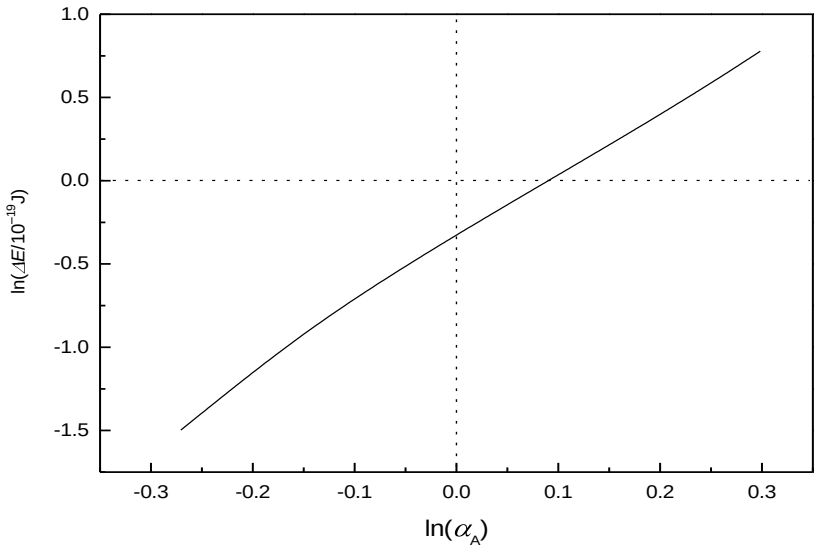

relevant in our calculations (see figure-3.7).

Figure- 3.7. Plot of ln($\Delta E/10^{-19}$J) with ln(α_A). The slope ≈4 .

Hence we take

$$\Delta E \propto (\alpha_A)^4 \tag{3.21}$$

Since ΔE linearly depends on the interaction parameter R_1, we assume that

$$R_1 = R_1^*(\alpha_A)^4 \tag{3.22}$$

where R_1^* is an input parameter. As will be discussed later (section 3.3.3.3 and section 3.4.2.3), inclusion of this variation of ΔE results in phase diagrams containing an N_R lake. Though the above calculation has been made for variation of chain length in a homologous series, the strong dependence of ΔE with respect to α_A appears to be valid only in case of mixtures of chemically dissimilar compounds which show the N_R lake in the temperature-concentration plane (see figure 3.4c). Mixtures of compounds belonging to the same homologous series show only SmA_1-SmA_d transition and not an N_R lake. R_2 can also be expected to depend weakly on the chain length in a homologous series *i.e.*, on the McMillan parameter α. We ignore this dependence of R_2 with α.

(7) As we have described in chapter-2, most experimental phase diagrams on binary mixtures of nematogens correspond to a negative deviation from the geometric mean (GM) approximation for the mutual interaction between the components and the deviation increases as the molecular structures of the two components become more dissimilar. Further, in chapter-2, we have shown that a negative deviation is necessary to get a nematic to nematic phase transition in polar compounds. We can expect a similar negative deviation in the mutual smectic interaction also, *i.e.*, for the McMillan parameter α_{AP}.

As we have discussed, the P-type and A-type configurations give rise to the SmA_1 and SmA_d phases respectively. There have been some experiments on binary mixtures of polar compounds [24] in which one component shows SmA_1 and the other shows SmA_d. In these cases, the smectic-nematic transition line has an appreciable concave shape, especially when the components have a large difference in the layer spacings, indicating a strong negative deviation from the GM approximation for the mutual interaction *i.e.*, $Q < 1$ in equation 3.19. As the chain length in a homologues series is

increased, the numerical value of α_A as also the structural dissimilarity between the P- and A-types of pairs is enhanced. Hence it is reasonable to assume that as α_A increases the deviation $|Q-1|$ from GM rule increases, or Q (<1)decreases. Since both α_A and α_P vary in a homologous series, we expect Q to depend on the ratio α_A/α_P (which is a rough measure of the dissimilarity) and we assume

$$Q = Q^* (\alpha_A/\alpha_P) \tag{3.23}$$

where Q^* is a constant chosen such that $Q < 1$ in the entire range of α_A used. Since α_P increases with the chain length more rapidly than α_A, the ratio α_A/α_P decreases moderately, and leads to results which can be compared with experimental data. For example, with $Q^* \approx 0.12$, we get $Q \approx 0.6$ for $\alpha_A \approx 0.4$ while $Q \approx 0.4$ for $\alpha_A \approx 1$.

In chapter-5, where a hybrid model is developed including the hard core interactions, we show that the excluded volume effects cause the *negative* deviation from the GM approximation and that the magnitude of the deviation increases as the two components become geometrically more dissimilar. In our present calculations where the hard core interactions are not taken into account, as in the previous chapter, the assumed negative deviation reflects the excluded volume effects.

3.3.1.2 Expressions for the free energy and the order parameters

Extending the McMillan theory to the case of mixtures and considering only the smectic interactions, the potential energy of the i^{th} A-type of pair can be written as

$$U_{Ai} = -U_0 X_A \alpha_A \tau_A \cos(2\pi z_{Ai}/d) - U_0 X_P \alpha_{AP} \tau_P \cos(2\pi z_{Ai}/d) \tag{3.24}$$

where X_A, X_P and τ_A , τ_P are the mole fractions and translational order parameters of the A- and P-types of pairs respectively, and d is the average layer spacing given by

$$d = X_A d_A + X_P d_P,$$

with $$d_A = r_0 + 2c$$

and $$d_P = r_0 + c. \tag{3.25}$$

Similarly for a P-type pair,

$$U_{Pj} = -U_0 X_P \alpha_P \tau_P \cos(2\pi z_{Pj}/d) - U_0 X_A \alpha_{PA} \tau_A \cos(2\pi z_{Pj}/d) \tag{3.26}$$

The internal energy of one mole of the pairs obtained by averaging over the distribution functions is

$$2U = \frac{NX_A}{2}\langle U_{Ai}\rangle + \frac{NX_P}{2}\langle U_{Pj}\rangle - NX_P\,\Delta E$$

$$= -\frac{N\,U_0}{2}\left[\,X_A{}^2\alpha_A\tau_A{}^2 + X_P{}^2\,\alpha_P\tau_P{}^2 + 2\alpha_E X_A\,X_P\tau_A\tau_P\right] - NX_P\,\Delta E \qquad (3.27)$$

where N is the Avogadro number, $\langle\ \rangle$ indicate statistical averages and the factor 2 on the left hand side reminds that we have a mole of pairs. The last term is the concentration dependent part of the configurational energy.

The molar entropy is given by

$$2\mathcal{S} = -N\,k_B\left[\,X_A\,\frac{1}{d}\int_{-d/2}^{+d/2} dz_{Ai}\,f_{Ai}\ln f_{Ai} + X_P\,\frac{1}{d}\int_{-d/2}^{+d/2} dz_{Pj}\,f_{Pj}\ln f_{Pj}\,\right]$$

$$-N\,k_B\left(\,X_A\ln X_A + X_P\ln X_P\,\right) \qquad (3.28)$$

where the last term is the entropy of mixing and f_A and f_P are the normalised translational distribution functions of A and P types of pairs respectively. The Helmholtz free energy is given by:

$$F = U - T\mathcal{S}. \qquad (3.29)$$

The normalised distribution functions f_A and f_P and the expression for X_A found by minimising F are,

$$f_{Ai}(z) = \frac{1}{Z_A}\exp(-U_{Ai}/k_BT) \qquad (3.30)$$

$$f_{Pj}(z) = \frac{1}{Z_P}\exp(-U_{Pj}/k_BT) \qquad (3.31)$$

and

$$X_A = \frac{1}{1 + \dfrac{Z_P}{Z_A}\exp(\Delta E/k_BT)} \qquad (3.32)$$

where Z_A and Z_P are the appropriate normalising integrals. The expressions for the smectic order parameters are given by,

$$\tau_A = \langle \cos(2\pi z_{Ai}/d)\rangle = \int_0^1 d\zeta_i \, f_{Ai}(z) \cos(\pi\zeta_{i\,A}) \tag{3.33}$$

$$\tau_P = \langle \cos(2\pi z_{Pj}/d)\rangle = \int_0^1 d\zeta_j \, f_{Pj}(z) \cos(\pi\zeta_{j\,P}) \tag{3.34}$$

where we have used the reduced coordinate $\zeta = 2z/d$.

3.3.1.3 Specific heat at constant volume

The molar specific heat at constant volume is give by

$$C_V = \left(\frac{\partial U}{\partial T}\right)_V$$

$$= -\frac{NU_0}{2}\left\{\frac{\partial X_A}{\partial T}[X_A\alpha_A\tau_A^{\,2} - X_P\alpha_P\,\tau_P^{\,2} + \alpha_E\tau_A\,\tau_P\,(X_P - X_A)]\right.$$

$$\left. + \frac{\partial \tau_A}{\partial T}[\,X_A^{\,2}\,\alpha_A\tau_A + \alpha_E\,X_AX_P\tau_P] + \frac{\partial \tau_P}{\partial T}[X_P^{\,2}\alpha_P\tau_P + \alpha_E X_AX_P\tau_A]\right\}$$

$$+ \frac{\partial X_A}{\partial T} N\Delta E. \tag{3.35}$$

Note that in the above expression, as explained in chapter-2, we have not differentiated ΔE with respect to T as it depends really on volume and the temperature dependence is taken only for convenience. Expressions for the derivatives of X_A, τ_A and τ_P are obtained by differentiating the relevant parameters in the equations 3.32, 3.33 and 3.34 respectively, with respect to T. We get,

$$\frac{\partial X_A}{\partial T}\left[\frac{U_0}{k_BT}(-\alpha_A\tau_A^{\,2} - \alpha_P\tau_P^{\,2} + 2\alpha_E\tau_A\tau_P) + \frac{1}{X_AX_P}\right]$$

$$+ \frac{\partial \tau_A}{\partial T}\left[\frac{U_0}{k_BT}(\alpha_E X_A\tau_P - \alpha_A X_A\tau_A)\right] + \frac{\partial \tau_P}{\partial T}\left[\frac{U_0}{k_BT}(\alpha_P X_P\,\tau_P - \alpha_E\,X_P\tau_A)\right]$$

$$+ \frac{U_0}{k_BT^2}[\alpha_A X_A\tau_A^{\,2} - \alpha_P X_P\tau_P^{\,2} + \alpha_E\tau_A\tau_P\,(X_P - X_A)] - \frac{\Delta E}{k_BT^2} = 0. \tag{3.36}$$

$$\frac{\partial X_A}{\partial T}\left[\frac{U_0}{k_B T}(\alpha_A \tau_A - \alpha_E \tau_P)\right] + \frac{\partial \tau_A}{\partial T}\left[\frac{U_0}{k_B T}\alpha_A X_A - \frac{1}{\Delta AS}\right] + \frac{\partial \tau_P}{\partial T}\left[\frac{U_0}{k_B T}\alpha_E X_P\right]$$

$$-\frac{U_0}{k_B T^2}[\alpha_A X_A \tau_A + \alpha_E X_P \tau_P] = 0. \qquad (3.37)$$

$$\frac{\partial X_A}{\partial T}\left[\frac{U_0}{k_B T}(\alpha_E \tau_A - \alpha_P \tau_P)\right] + \frac{\partial \tau_A}{\partial T}\left[\frac{U_0}{k_B T}\alpha_E X_A\right] + \frac{\partial \tau_P}{\partial T}\left[\frac{U_0}{k_B T}\alpha_P X_P - \frac{1}{\Delta PS}\right]$$

$$-\frac{U_0}{k_B T^2}[\alpha_P X_P \tau_P + \alpha_E X_A \tau_A] = 0. \qquad (3.38)$$

where, we have used,

$$\Delta AS = \langle [\cos(2\pi z_{Ai}/d)]^2 \rangle - \tau_A^2$$

$$\text{and} \quad \Delta PS = \langle [\cos(2\pi z_{Pj}/d)]^2 \rangle - \tau_p^2 \qquad (3.39)$$

The relevant derivatives are obtained by solving the three simultaneous equations 3.36, 3.37 and 3.38 and used to calculate C_V.

3.3.2 Method of calculation

The smectic interaction parameter is assumed to be $U_0\alpha$ with $U_0 = 4.541\times500k_B$ *i.e.*, $T^* = 500$K, which corresponds numerically to the value of T_{NI} used in the previous chapter. We use $Q < 1$ *i.e,* $\alpha_E < \sqrt{\alpha_A \alpha_P}$ in equation 3.19 to take into account the negative deviation from the GM approximation. At any reduced temperature T_R, consistent values of τ_A and τ_P are found as X_A is varied from 0 to 1 for the assumed set of the four parameters of the problem, *viz.* R_1^*, R_2, α_A, and Q^*. The free energy is calculated in each case. Near the minimum of F with respect to X_A, equation 3.32 is used to find the consistent value of X_A. We usually get more than one set of self consistent values of X_A , τ_A and τ_p. The stable solution corresponds to the one with the lowest value of F. Calculations have been made for $R_1^*=8$ and R_2 around 0.7 which are very reasonable values as described in chapter-2. We evaluate all the necessary integrals numerically using a 32 point Gaussian quadrature method in double precision.

We look for the following types of solutions:

(i) $\tau_A = \tau_P = 0$ corresponding to the nematic phase, and,

(ii) $\tau_A \neq \tau_P \neq 0$ corresponding to smectic phase which is SmA_1 if X_A is relatively small and SmA_d if X_A is relatively large.

3.3.3 Results and discussion

Depending on the values of the parameters used, our calculations give the following results: (i) a first order SmA_1 -SmA_d transition changing to a continuous SmA_1 to SmA_d evolution beyond a critical point (ii) a re-entrant nematic lake associated with the SmA_1 -SmA_d transition, and (iii) the re-entrant nematic lake merging with the nematic sea. We discuss these in the following subsections.

3.3.3.1 First order SmA_1-SmA_d transition ending in a critical point

Since the SmA_1 and the SmA_d phases have the same symmetry, we can expect a first order SmA_1-SmA_d transition or a continuous evolution of SmA_1 to SmA_d beyond a critical point. The temperature-α_A phase diagram obtained with $Q^* = 0.22$ and $R_2 = 0.7$ is shown in figure 3.8. Keeping R_1^* and R_2 fixed, if a lower value of Q is used, *i.e.*, the deviation from the GM rule is slightly larger, the critical point C_1 of the SmA_1-SmA_d transition is shifted to a lower value of α_A while the rest of the diagram does not change perceptibly. This is shown by a dashed line in figure 3.8 for $Q^* = 0.2$ for which the critical point is at $\alpha_A = 0.945$ and $T_R = 0.60867$.

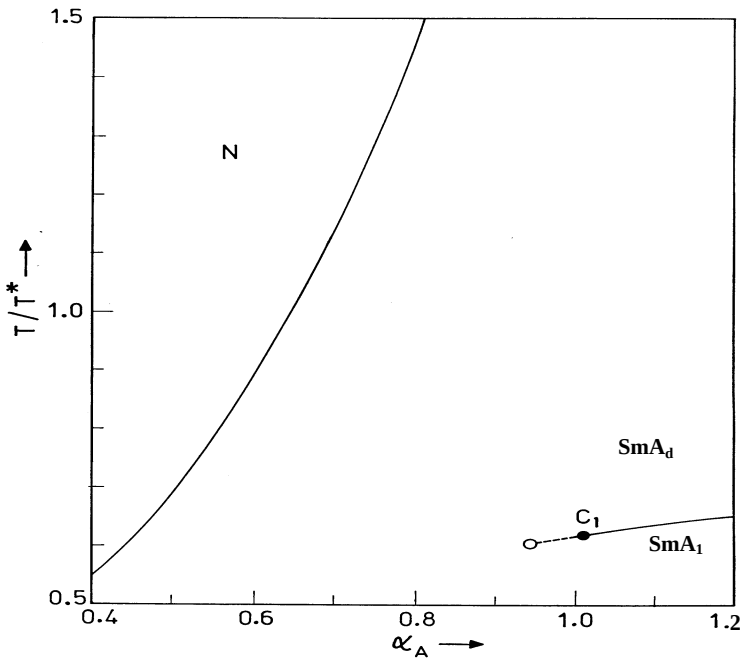

Figure – 3.8. Calculated phase diagram showing the SmA_1-SmA_d critical point C_1 for $R_1^* = 8$, $R_2=0.7$ and $Q^* =0.22$. The open circle shows the critical point which is shifted to a lower value of α_A when $Q^* = 0.2$. The rest of the diagram does not change perceptibly when Q^* is reduced from 0.22 to 0.2.

It can be seen that the first order SmA_1- SmA_d boundary ends at a critical point C_1 as α_A is decreased. This can be understood as follows. For low values of α_A, the free energy has a single minimum with respect to X_A. For higher values of α_A, the structural dissimilarity between the A-type of pairs and the P-type of pairs is large, leading to a large negative deviation from GM rule (see equation 3.23), *i.e.*, the mutual interaction between the A-type of pairs and the P-type of pairs is relatively weak. Hence the 'middle' concentrations (*i.e.*, $X_A \approx 0.5$) are not favoured and this causes a 'hump' in the variation of the free energy with respect to X_A resulting in *two* minima. This is shown in figure 3.9 for α_A =1.1. At $T_R \approx 0.6383$, the two minima in free energy become equal resulting in a first order SmA_1-SmA_d transition with a jump in X_A. The latter along with the jumps in the order parameters are shown in figure 3.10. In the narrow range of temperatures around $T_{A1\text{-}Ad}$ shown in the figure 3.10, the order parameter τ_P does not have an appreciable dependence on temperature. Over a wider range, τ_P generally decreases with increase of temperature.

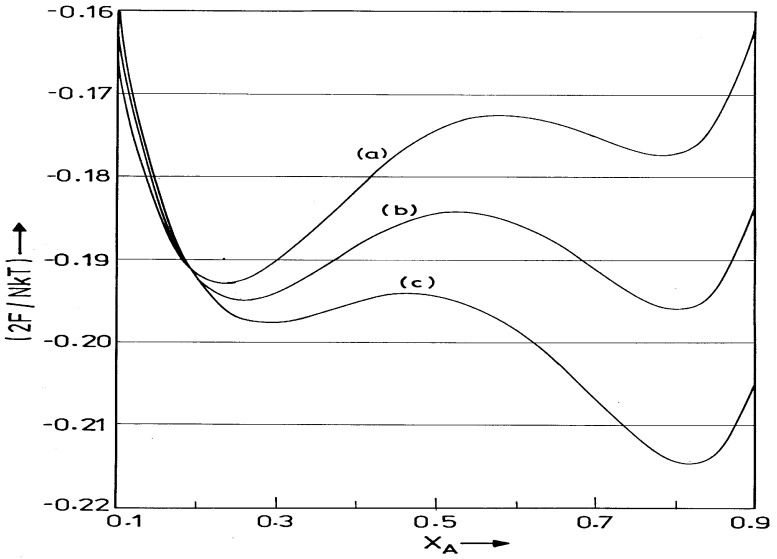

Figure – 3.9. Molar Helmholtz free energy difference ($F_{\text{smectic}} - F_{\text{nematic}}$) as a function of relative concentration of the A-type of pairs (X_A) at three temperatures near $T_{A1\text{-}Ad}$ for $R_1^* = 8$, $R_2 = 0.7$, $Q^* = 0.22$ and $\alpha_A = 1.1$ (a)T/T^*=0.6373 (b) T/T^* =0.6383 and (c) $T/T^* = 0.6393$.

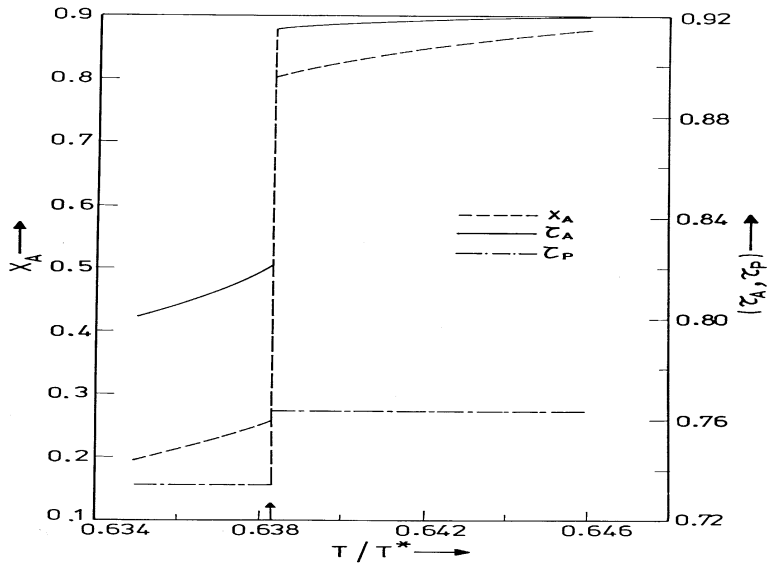

Figure – 3.10. Relative concentration of the A-type of pairs (X_A), smectic order parameter for the A-type of pairs (τ_A) and for P-type of pairs (τ_P) as functions of T/T^* near $T_{A1\text{-}Ad}/\ T^* = 0.6383$. Other parameters are the same as in figure 3.9.

As α_A is decreased, the dissimilarity between the A- and P-types of pairs is reduced. Hence the SmA_1-SmA_d transition becomes weaker and at a specific value of α_A (≈ 1.01) the first order SmA_1-SmA_d line ends in a critical point C_1 for $T_R = 0.62238$ (see figure 3.8). As the critical point is reached, as expected, the jumps in X_A, τ_A, τ_P and the internal energy approach zero (figure 3.11).

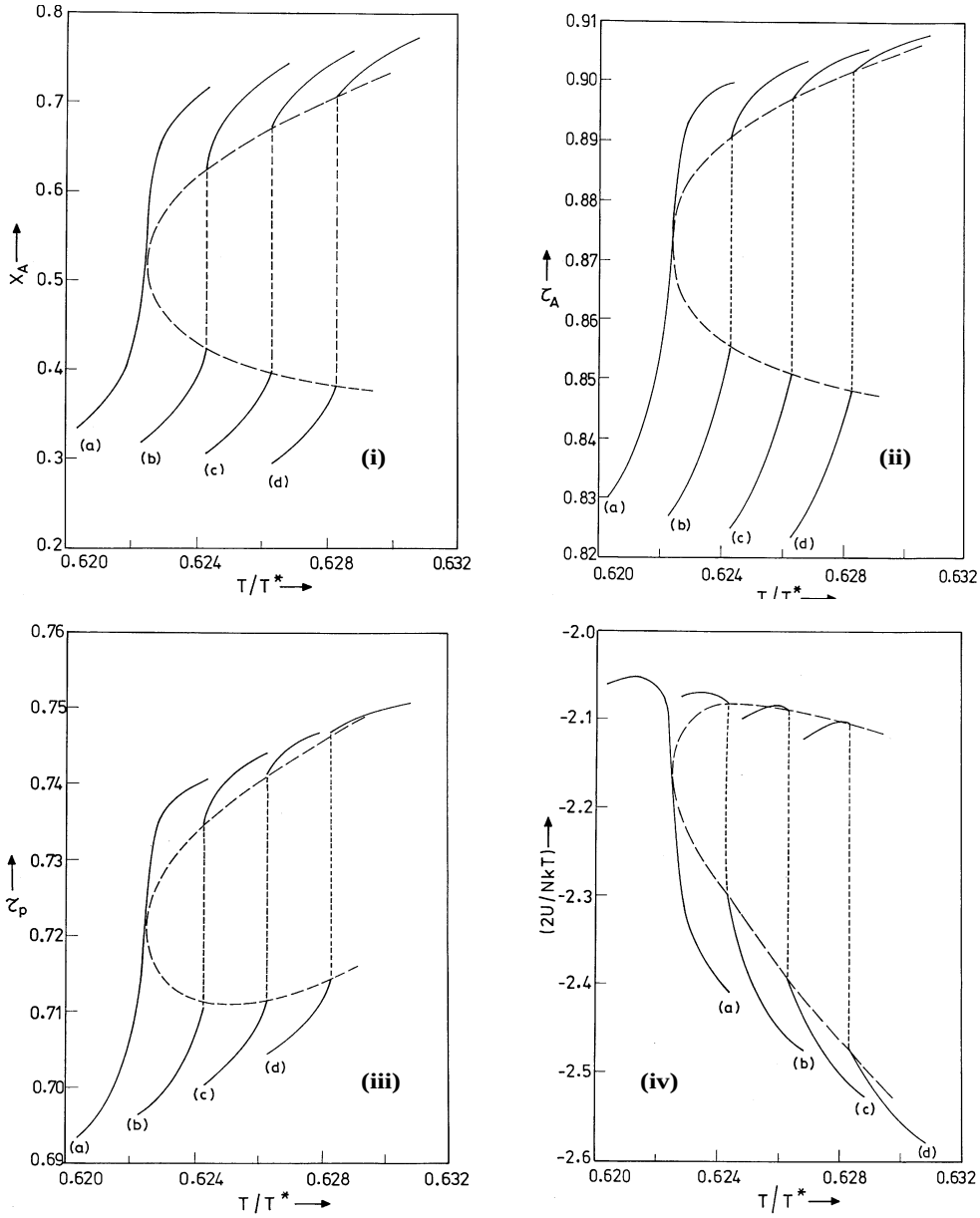

Figure – 3.11. (i) Relative concentration of the A-type of pairs (X_A), (ii)smectic order parameter of the A-type of pairs (τ_A), (iii) smectic order parameter of the P-type of pairs (τ_P) and (iv) internal energy per mole of pairs ($2U$) as functions of T/T^* near the critical point C_1 of figure 3.8 for $R_1^* = 8$, $R_2 = 0.7$, $Q^* = 0.22$ and (a) $\alpha_A = 1.01$, (b) $\alpha_A = 1.02$, (c) $\alpha_A = 1.03$, (d) $\alpha_A = 1.04$.

Over a narrow range of temperatures close to the critical point, the value of X_A increases rapidly with temperature. As X_A increases, the effective smectic interaction potential of the A-type of pairs ($X_A\alpha_A$) and the mutual interaction ($X_A\alpha_{AP}$) increase. This results in an increase of both τ_A and τ_P with temperature. However, over a wider range of temperatures, τ_A and τ_P generally decrease as the temperature is increased.

This variation is similar to that in the average orientational order parameter near the N_1-N_d transition for Y <1 (*i.e.*, the orienting potential of the P-type pairs less than that of the A-type of pairs) discussed in chapter-2 (see section 2.4.3.3 and figures 2.16 and 2.17).

As the critical point is reached, the specific heat (C_V) peak becomes stronger and finally diverges as shown in figure 3.12. Note that C_V shown in figure 3.12 is obtained as $\left(\frac{\partial U}{\partial T}\right)_V$ *without* differentiating ΔE with respect to T (see section 3.3.1.3), while the variation of U shown in figure 3.11(iv) includes the variation of ΔE with respect to T.

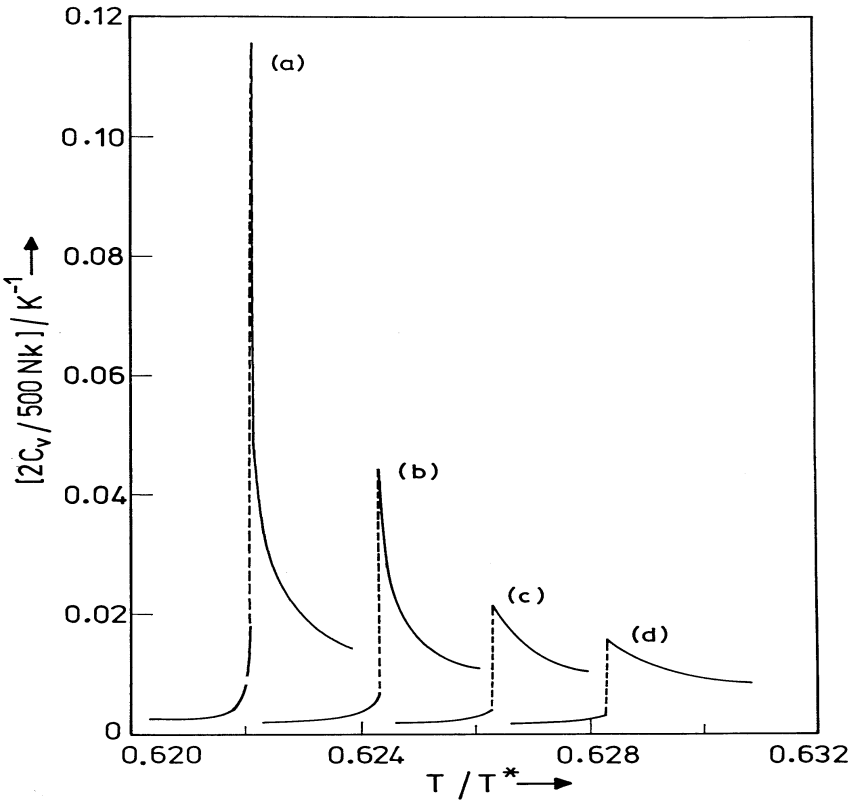

Figure – 3.12. Specific heat at constant volume per mole of pairs ($2C_v$) as a function of T/T^* near the critical point C_1 of figure 3.18. The parameters corresponding to (a) ,(b), (c) and (d) are the same as in figure 3.11

3.3.3.2 Two SmA_1-SmA_d transition lines ending in critical points C_1 and C_2

A further lowering of Q results in other interesting results. With $Q^* = 0.19$, we have extended the calculations for α_A values much lower than that corresponding to C_1. At some low value of α_A, the SmA_1-SmA_d transition *reappears* below another

critical point C_2 (see figure 3.13). This indicates that, at low values of T_R and α_A, the free energy again has two *equal* minima with respect to X_A. This can be understood as follows.

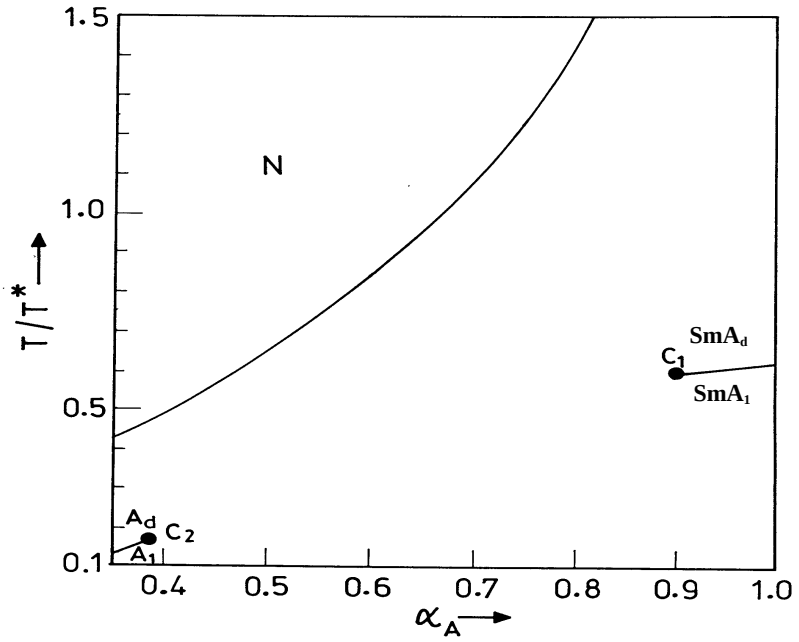

Figure – 3.13. Calculated phase diagram showing two SmA_1-SmA_d critical points C_1 and C_2 for $R_1^* = 8$, $R_2 = 0.7$, and $Q^* = 0.19$. Near C_2, SmA_1 and SmA_d are denoted as A_1 and A_d respectively.

It can be seen from figure 3.14 that, for higher values of α_A, a steep variation of X_A with T_R occurs at $T_R \approx R_2$, whereas when α_A has a low value, it occurs at T_R considerably lower than R_2.

ΔE varies as α_A^4 (see equation 3.21) and at any given value of T_R, ΔE is very low for low values of α_A. Further, when α_A is decreased, α_P decreases more rapidly than α_A and hence the ratio α_A/α_P (which is > 1) is large thus favouring the A-type configuration. Hence X_A is relatively large even when T_R is much less than R_2. However, as the temperature is further decreased, ΔE becomes sufficiently strong to lower the value of X_A.

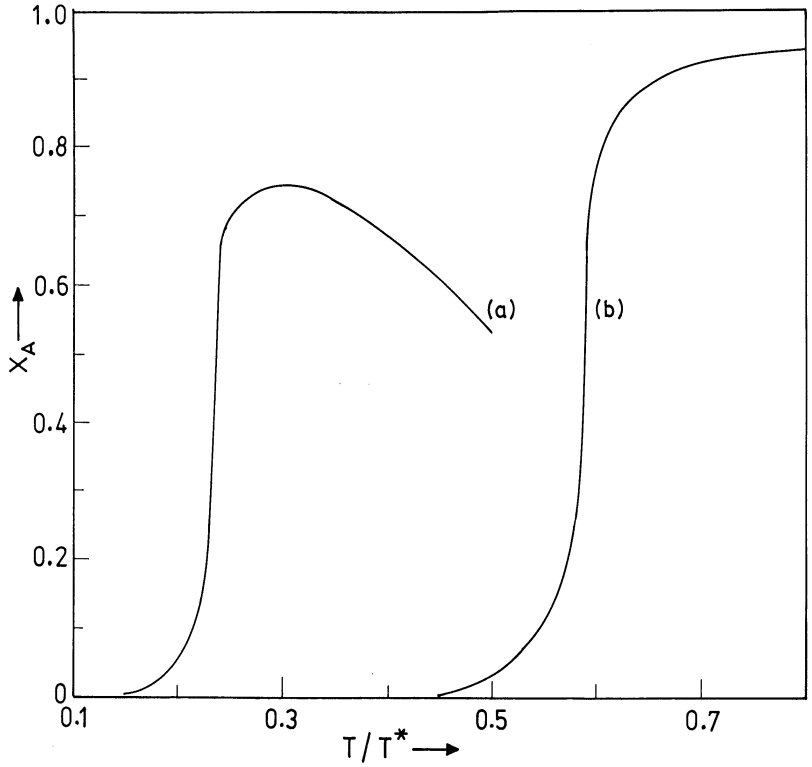

Figure – 3.14. Relative concentration of the A-type of pairs (X_A) plotted as a function of T/T^* for $R_1^* = 8$, $R_2 = 0.7$, $Q^* = 0.18$ and (a) $\alpha_A = 0.43$, (b) $\alpha_A = 0.865$. Note that in (a), the rather low value of ΔE leads to a significant *decrease* in X_A as T/T^* is increased beyond 0.3.

Since ΔE is small for low values of α_A, even though X_A has a steep variation, the free energy does not vary much over a wide range of X_A (see equations 3.27 and 3.29). Hence, for lower values of α_A, the free energy has a flat minimum with respect to X_A (see figure 3.15) while it has a deeper minimum for larger values of α_A. Therefore, at low values of α_A, even a small negative deviation from GM rule is sufficient to cause a 'hump' in the free energy minimum, resulting in *two minima* with respect to X_A. This leads to SmA_1-SmA_d transition. Thus, even though the deviation from the GM rule (*i.e*, $|Q - 1|$) *decreases* as α_A is decreased (see equation 3.23 and figure 3.15), the SmA_1-SmA_d transition reappears below some values of α_A, *i.e*., below another critical point C_2. If the negative deviation from GM rule is stronger (*i.e*, as Q is lowered), the critical point C_2 is shifted to higher value of α_A and T_R. For $Q^* = 0.19$, C_2 is at $\alpha_A = 0.385$ and $T_R \approx 0.1693$ (figure 3.13). For $Q^* = 0.18$, C_2 is at $\alpha_A \approx 0.43$ and $T_R \approx 0.2316$ as indicated by vanishing of two minima(figure 3.15).

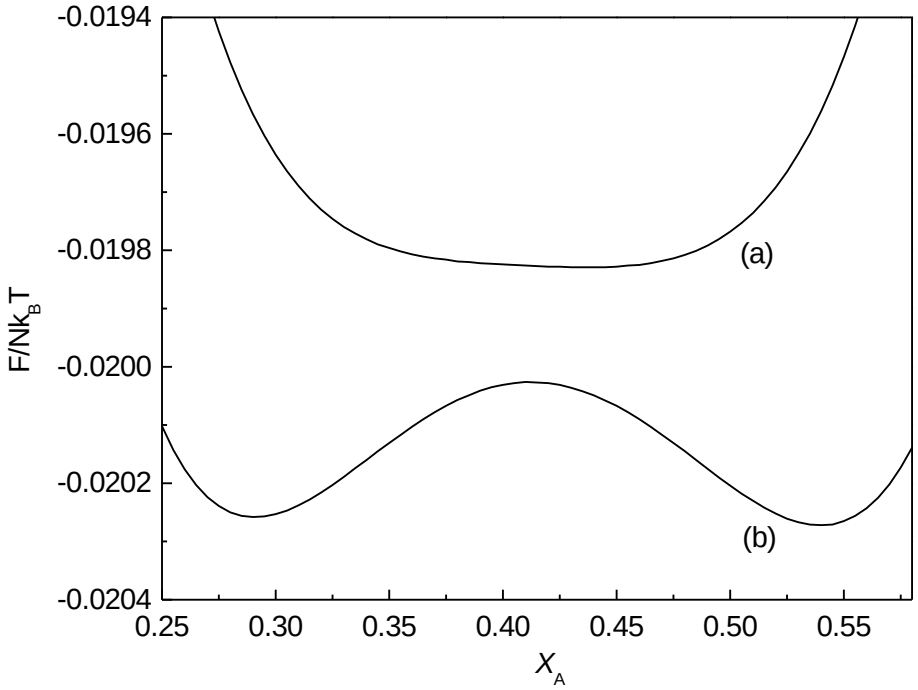

Figure – 3.15. Variation of free energy as a function of X_A for two values of α_A near the critical point C_2, with $R_1^* = 8$, $R_2 = 0.7$, $Q^* = 0.18$ and (a)$\alpha_A = 0.43$, $T_R = 0.2316$ (b) $\alpha_A = 0.42$, $T_R = 0.2178$. Note that the value of Q is 0.9132 for (a) and 0.9234 for (b) (see equation 3.23).

In general as Q^* is lowered, both C_1 and C_2 approach each other. For a sufficiently low value of Q^* we can expect them to merge. But, much before this happens, a nematic lake appears in the middle which is discussed in the next subsection.

3.3.3.3 Re-entrant nematic lake

When Q^* is 0.188, the nematic phase just re-enters over narrow ranges of α_A (between 0.585 and 0.593) and temperature (T_R between 0.352 and 0.358). On lowering Q^* to 0.18, the N_R region widens as a lake occupying larger ranges of α_A and temperature (figure 3.16).The appearance of the N_R can be understood as follows.

In a binary mixture of polar compounds, since the ΔE values of the components are different, the average ΔE per pair can be expected to change with composition. As explained earlier, in our model, α_A is taken to represent a given concentration and ΔE is assumed to vary as α_A^4. Therefore, ΔE is very low for small values of α_A. But, in our model, the re-entrance of the nematic phase on cooling is due to the rapid changeover of A-type of pairs to P-type of pairs at a temperature not low enough to

stabilise the SmA_1 phase. However, when ΔE is very low, as discussed in the previous subsection, and shown in figure 3.14, this changeover occurs at temperatures low enough for the SmA_1 phase to be stable. Therefore, as the temperature is varied at low values of α_A, the smectic phase is stable without the intervening N_R region. On the other hand, at intermediate value of α_A, ΔE is strong enough to bring about the 'A' to 'P' changeover at a *higher temperature*, thus resulting in double re-entrance.

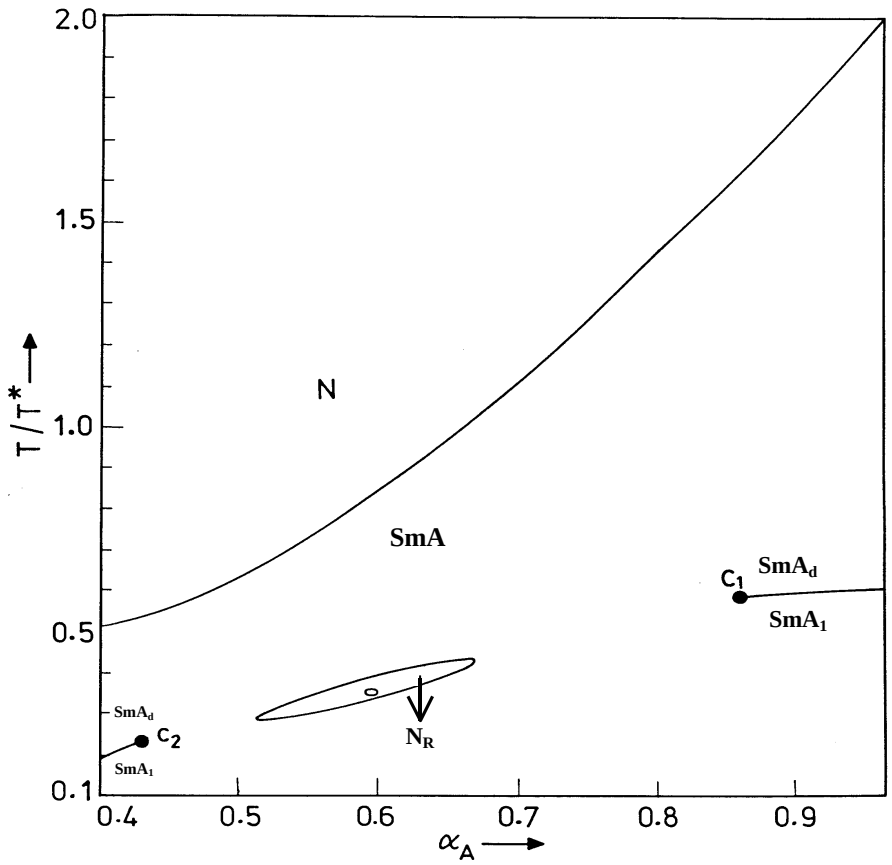

Figure – 3.16. Calculated phase diagram for $R_1^* = 8$, $R_2 = 0.7$ showing the re-entrant nematic (N_R) lake for $Q^* = 0.18$. C_1 and C_2 are the SmA_1-SmA_d critical points. The small loop within the N_R lake is for $Q^* = 0.188$, for which the N_R lake just appears.

Larger values of α_A also lead to larger values of α_p. Hence the SmA phase is stable even when X_A is small, leading again to the disappearance of the N_R phase. Hence, the N_R region appears as a *lake* over a range of *intermediate* values of α_A or equivalently, over a range of intermediate concentrations in a mixture. In general, we can see that, in the presence of a strong negative deviation from GM rule, the smectic phase is destabilised in the 'middle' concentrations, whereas the 'pure' components have only smectic phases. Indeed, experiments [6, 11, 25] on binary mixtures show

that the N_R-lake appears around a concentration of 50 %. Further, the N_R- lake appears in association with SmA_1-SmA_d boundary in the experimental studies also (for example, see figure 3.4c above).

A further increase of the negative deviation ($Q^* = 0.15$) obviously widens the N_R lake and also as discussed earlier, brings the critical points C_1 and C_2 closer (figure 3.17a). In this case, near the extreme values of α_A the N_R phase occurs below the SmA_d-SmA_1 transition line. For still lower value of Q ($Q^* = 0.12$, see figure 3.17b) or when ΔE is increased using a higher value of $R_2 = 0.72$, (see figure 3.18a), the N_R-lake becomes still wider and swallows one or both the SmA_1-SmA_d critical points.

When ΔE is increased further, the nematic lake becomes much wider and eventually merges with the nematic sea creating a 'nematic gap' over a range of α_A values (figure 3.18b). Obviously, the nematic gap widens as Q^* is further decreased or equivalently, the components in a binary mixture become structurally more dissimilar. This agrees with the appearance and widening of the nematic gap in experiments [24] on binary mixtures of 8OCB with one of the homologues of *n*DBT (*n* alkyl isothiocyanatophenyl dioxane) exhibiting SmA_d and SmA_1 phases respectively. With the lower values of *n*, the components have larger ratio of smectic layer spacing and are structurally more dissimilar. For mixtures of 8OCB and 7DBT, the layer spacing ratio r = 1.46 and the nematic gap is over a small concentration range of $X = 0.4$ to 0.75 of 8OCB, whereas for mixtures of 8OCB and 4DBT, r = 1.76 and the nematic gap is wider, between $X = 0.3$ to 0.9 [24]. Also, we note that the calculated N-SmA_d-N_R boundary is parabolic (figure 3.18b) as seen in the experimental phase diagrams [24].

Experimentally it is possible to measure the temperature variation of the smectic layer spacing. We plot in figure 3.19 the calculated values of the relative layer spacing

$$d/d_P = (X_A d_A + X_P d_P)/d_P \qquad (3.40)$$

as functions of relative temperature for three values of the McMillan parameter α_A corresponding to the phase diagram shown in figure 3.17a. Note that d shows a maximum value as the temperature is increased in the SmA_d phase. This trend reflects the temperature variation of X_A (see figure 3.14). The increase in layer spacing from SmA_1 to SmA_d has been experimentally measured [19].

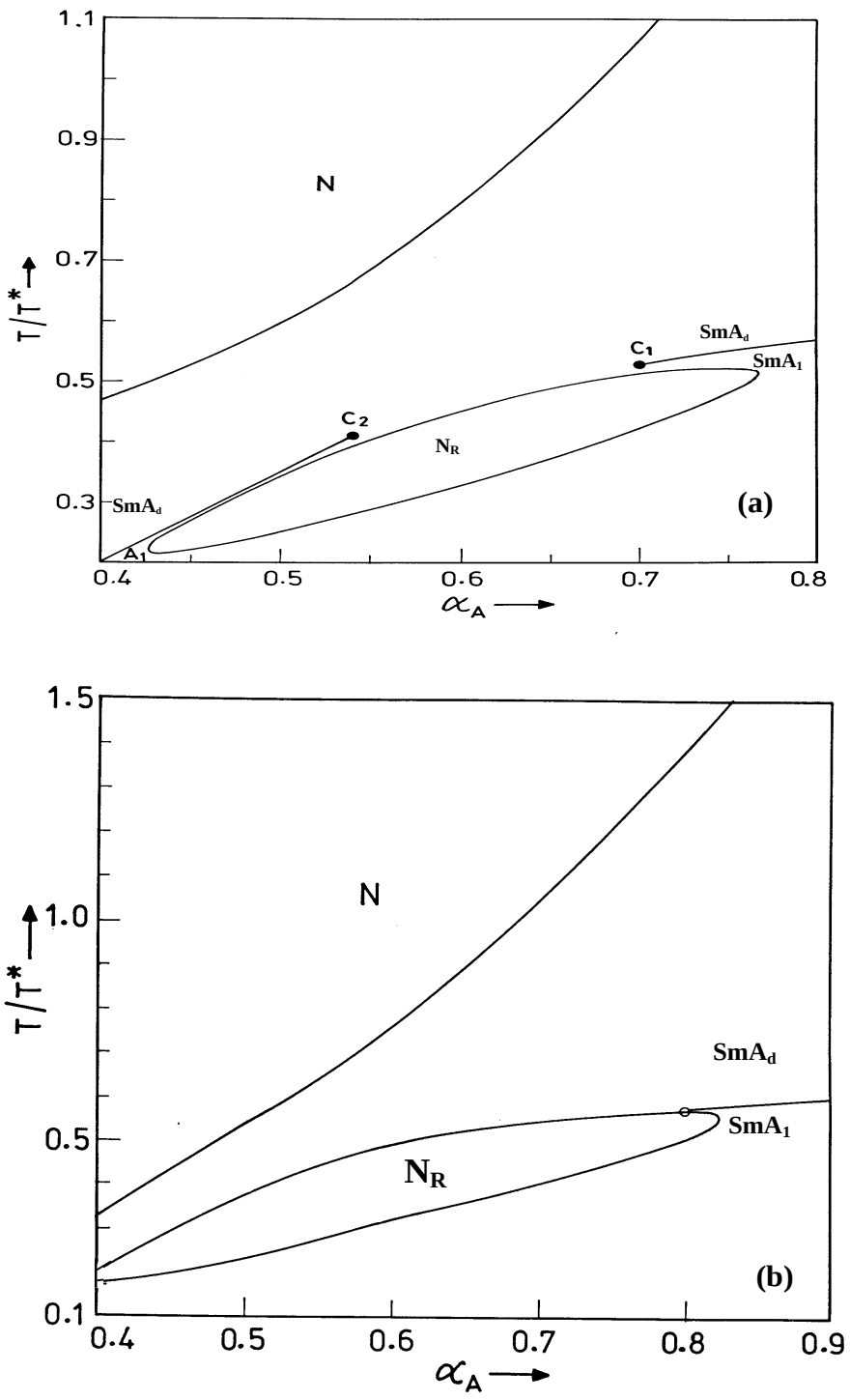

Figure- 3.17. Calculated phase diagram showing a wide re-entrant nematic (N_R) lake for R_1^* =8, R_2 = 0.7 . (a) Q^* = 0.15. C_1 and C_2 are the SmA_1-SmA_d critical points. SmA_1 is indicated as A_1 at the bottom left corner of the figure. (b) Q^* = 0.12. The point where first-order SmA_1-SmA_d transition line meets the boundary of N_R lake is shown by the open circle.

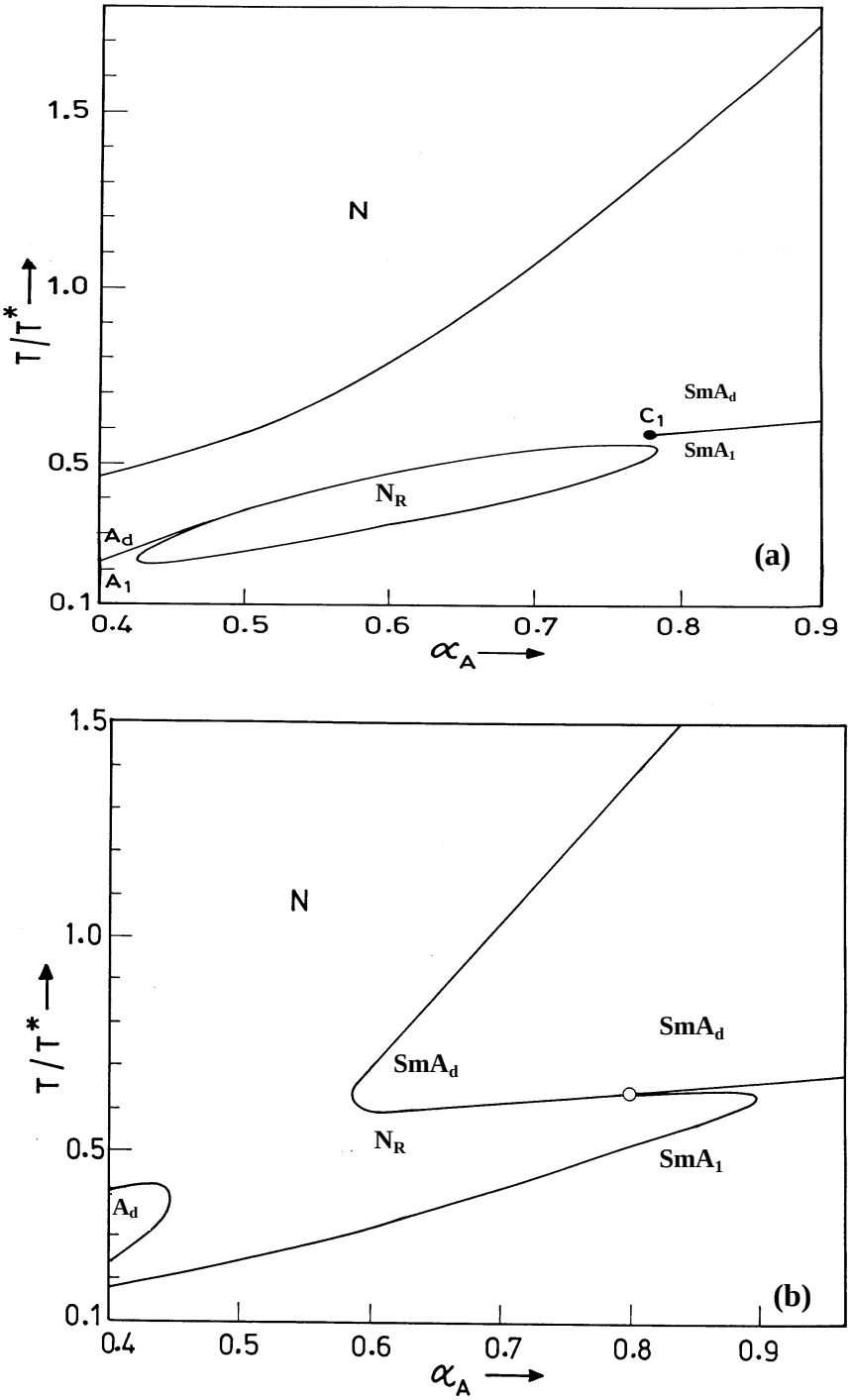

Figure –3.18. (a) Calculated phase diagram showing a wide re-entrant nematic (N_R) lake for R_1* =8, R_2 =0.72 and Q* = 0.15. In this case, the first order SmA_1-SmA_d transition line merges with the boundary of the lake in the lower range of α_A. (b) Calculated phase diagram showing the re-entrant nematic (N_R) lake merging with the nematic sea creating a nematic gap, for R_1* = 8, R_2 = 0.75, Q* = 0.12. The open circle indicates the point where the SmA_1-SmA_d transition line meets the N_R boundary. In some parts of the figures, SmA_1 and SmA_d are indicated as A_1 and A_d respectively.

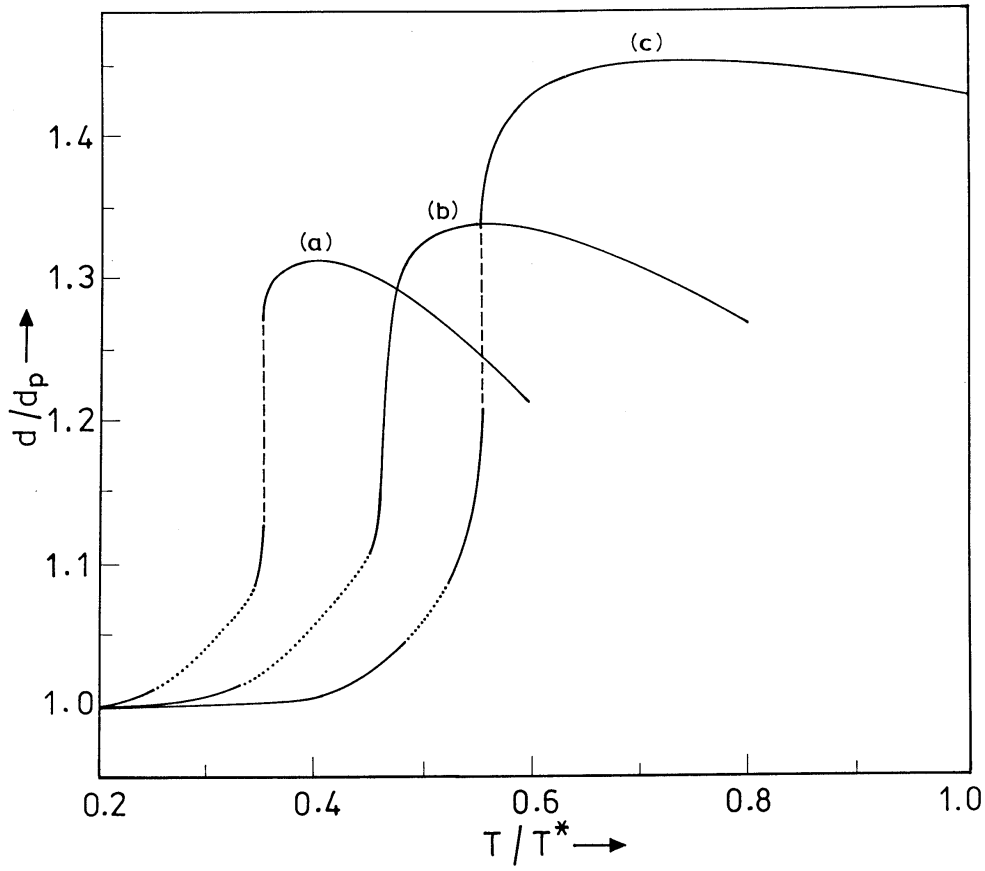

Figure – 3.19. The ratio of average layer spacing *d* to the molecular length d_P as a function of T/T^* for (a) α_A = 0.5, (b) α_A =0.6 and (c) α_A = 0.75 corresponding to the phase diagram of figure 3.17a. The dotted lines in the N_R phase represent the *d* values of smectic like short range order. The dashed lines indicate jumps in *d* at the first order SmA_1-SmA_d transitions.

3.3.3.4 Comparison with other theoretical models

The dislocation loop melting theory developed by Prost and Toner [17] predicts different types of topologies showing a first order SmA_1- SmA_d transition boundary ending at a critical point, the N_R-lake associated with SmA_1-SmA_d transition and the N_R -lake merging with the main nematic sea as shown in figures 3.5 and 3.6. These topologies are similar to those obtained by our theoretical calculations. Note that, figure 3.6 shows a nematic-nematic transition also. As described in the previous chapter (see chapter-2, section 2.4.3), taking into account only the orientation dependent part of the interactions, a nematic-nematic transition can be obtained *only if* we assume a negative deviation from the geometric mean (GM) rule for the mutual

orienting potential. But, in the present calculations such a transition is not possible since the nematic order is taken to be saturated. In the next section, we extend the theory to include an unsaturated nematic order and discuss the results. The microscopic theory using the frustrated spin-gas model developed by Berker *et.al* [26] predicts the possibility of double re-entrance, quadruple re-entrance, SmA_1- SmA_d transition, N_R -lake surrounded by the SmA_d region *etc*. However, as noted by Garland *et al* [27], the N_R-lake predicted by the frustrated spin-gas model does not occur in association with the SmA_1-SmA_d transition whereas the experiments [25, 27] and also the Landau theory by Prost and Toner [17] indicate that the N_R-lake occurs in association with the SmA_1-SmA_d transition line and eventually replaces the SmA_1-SmA_d critical point. This feature is brought out in our molecular model. However, the predicted temperature range of N_R-lake is much larger than the experimental one.

We now extend the theory to include the orientational interactions also.

3.4 Extension of the theory to include unsaturated nematic order

In the previous section, we have developed a theory of smectic mixtures to describe the SmA_1 -SmA_d transition assuming a saturated nematic order is, *i.e.*, $S = 1$. Depending on the values of the parameters used, our calculations have shown the possibility of (i) a first order SmA_1 -SmA_d transition changing to a continuous SmA_1 to SmA_d evolution beyond a critical point (ii) a re-entrant nematic lake associated with the SmA_1 -SmA_d transition, and (iii) the re-entrant nematic lake merging with the nematic sea.

In chapter-2, we have described the nematic-nematic transition considering only the orientational interactions. The nematic-nematic transition found experimentally in a system [28] occurs in the reentrant nematic range associated with SmA_1-SmA_d transition. In order to describe this feature, we extend our model to include both the nematic and smectic interactions. In the next section, the theoretical model is presented.

3.4.1 Theoretical model

3.4.1.1 Assumptions

We have made the following modifications of our assumptions mentioned in section 3.3.1.1.

(1) As explained in chapter-2, The energy difference between the A and P type configurations is written in terms of the N-I transition temperature T_{NI}

$$\Delta E = E_A - E_P = R_1 k_B T_{NI}\left(\frac{R_2}{T_R} - 1\right) \tag{3.41}$$

(2) Since the A and P type of pairs are geometrically dissimilar, as in chapter-2, we assume that the orientational potential for A-type of pairs U_{AA} and P-type of pairs U_{PP} to be different. We write,

$$U_{PP} = Y\, U_{AA} \tag{3.42}$$

and the mutual interaction potential

$$U_{AP} = U_{PA} = P\sqrt{U_{AA}\, U_{PP}} \tag{3.43}$$

where $P \neq 1$ indicates a deviation from the geometric mean (GM) rule in the orientational part of the mutual interaction potential.

(3) Following Kventsel *et al* [29], we decouple the translational and orientational parts in the McMillan's 'mixed' order parameter (σ) and write

$$\sigma = \langle P_2(\cos\theta)\rangle \langle \cos(2\pi z/d)\rangle$$

$$i.e., \quad \sigma = S\tau \tag{3.44}$$

(4) As explained in section 3.3.1.1, a negative deviation from the geometric mean (GM) approximation for the mutual interaction between the components can be assumed to be valid. Hence we can assume both P and Q to be < 1. The deviation increases as the molecular structures of the two components in a mixture become more dissimilar. As the chain length in a homologues series is increased, the numerical value of α_A and also the structural dissimilarity between the P-and A-types of pairs is enhanced. Hence it is reasonable to assume that, as α_A increases, the deviations ($|1-P|$ and $|1-Q|$) from GM approximation increase, or P and Q decrease.

Since P and Q always occur together in the expressions involving the mutual interaction in all the equations, it is enough to consider the variation of P with respect to α_A, *i.e.*, we do not use the equation 3.23 above. Since both α_A and α_P vary in a homologous series, as explained earlier, we expect P to depend on the ratio α_A/α_P and we assume, as in equation 3.23

$$P = P^* (\alpha_A/\alpha_P) \tag{3.45}$$

where P^* is a constant chosen such that $P < 1$ in the entire series.

3.4.1.2 Free energy and order parameters

The medium is assumed to consist of a *mixture* of A-type pairs and P-type pairs. Extending the McMillan theory to the case of mixtures, the potential energy of the i^{th} A-type of pair can be written as

$$U_{Ai} = -U_{AA} X_A S_A P_2(\cos\theta_{Ai})[1 + \alpha_A \tau_A \cos(2\pi z_{Ai}/d)]$$
$$- U_{AP} X_P S_P P_2(\cos\theta_{Ai})[1 + \alpha_{AP} \tau_P \cos(2\pi z_{Ai}/d)] \tag{3.46}$$

where X_A, X_P, S_A, S_P and τ_A ,τ_P are the mole fractions, orientational and translational order parameters of A and P types of pairs respectively and d the average layer spacing (see equation 3.25). Similarly for a P-type pair, U_{pj} is obtained by interchanging suffixes A and P in equation 3.46. Now, the internal energy of one mole of pairs can be written as

$$2U = \frac{NX_A}{2}\langle U_{Ai}\rangle + \frac{NX_P}{2}\langle U_{Pj}\rangle - NX_P \Delta E$$

$$= -\frac{N U_{AA}}{2}[X_A^2 S_A^2 (1+\alpha_A \tau_A^2) + Y X_P^2 S_P^2 (1+\alpha_P \tau_P^2) + 2P\sqrt{Y} X_A X_P S_A S_P(1+\alpha_E \tau_A \tau_P)]$$

$$- NX_P \Delta E \tag{3.47}$$

where we have used the equations 3.42, 3.43 and the factor 2 on the left hand side reminds that we have a mole of pairs. We have also added the concentration dependent part of the configurational energy.

The molar entropy is given by:

$$2\mathcal{S} = -N k_B \left[X_A \frac{1}{d} \int_{-d/2}^{+d/2} dz_{Ai} \int_0^1 d(\cos\theta_{Ai})\, f_{Ai} \ln f_{Ai} + X_P \frac{1}{d} \int_{-d/2}^{+d/2} dz_{Pj} \int_0^1 d(\cos\theta_{Pj})\, f_{Pj} \ln f_{Pj} \right]$$

$$- N k_B (X_A \ln X_A + X_P \ln X_P) \qquad (3.48)$$

where the last term is the entropy of mixing and f_A and f_P are the normalised distribution functions of A and P type of pairs respectively. The Helmholtz free energy is given by:

$$F = U - T\mathcal{S} \qquad (3.49)$$

The distribution functions f_A and f_P are found by minimising F. It can be shown that [29] the decoupling assumption (see equation 3.44) leads to the result

$$f_A = f_{Ao}\, f_{At} \text{ , and } f_P = f_{Po}\, f_{Pt} \qquad (3.50)$$

where f_{Ao} and f_{At} are the orientational and translational distribution functions of the A-type of pairs and f_{Po} and f_{Pt} are similar functions for the P-type of pairs. We have

$$f_{Ao} = \frac{1}{Z_{Ao}} \exp\left\{ \frac{U_{AA}}{k_B T} [\, X_A S_A (1+\alpha_A \tau_A^2) + P\sqrt{Y}\, X_P S_P (1+\alpha_E \tau_A \tau_P)] P_2(\cos\theta_A) \right\}$$

$$f_{Po} = \frac{1}{Z_{Po}} \exp\left\{ \frac{U_{AA}}{k_B T} [\, Y X_P S_P (1+\alpha_P \tau_P^2) + P\sqrt{Y}\, X_A S_A (1+\alpha_E \tau_A \tau_P)] P_2(\cos\theta_P) \right\}$$

$$f_{At} = \frac{1}{Z_{At}} \exp\left\{ \frac{U_{AA}}{k_B T} S_A [\alpha_A X_A S_A \tau_A + P\sqrt{Y}\, \alpha_E X_P S_P \tau_P] \cos(2\pi z_A/d) \right\}$$

$$f_{Pt} = \frac{1}{Z_{Pt}} \exp\left\{ \frac{U_{AA}}{k_B T} S_P [Y\alpha_P X_P S_P \tau_P + P\sqrt{Y}\alpha_E X_A S_A \tau_A] \cos(2\pi z_P/d) \right\} \qquad (3.51)$$

where Z_{Ao}, Z_{Po}, Z_{At} and Z_{Pt} are the corresponding normalising integrals. The order parameters are given by:

$$S_A = \int_0^1 d(\cos\theta_{Ai}) P_2(\cos\theta_{Ai})\, f_{Ao} \qquad (3.52)$$

and

$$\tau_A = \int_0^1 d(\zeta_A) \cos(\pi\zeta_A)\, f_{At} \qquad (3.53)$$

where the reduced co-ordinate $\zeta_A = (2z_A/d)$ is used. S_P and τ_P are obtained by interchanging the suffixes A and P in equations 3.52 and 3.53.

The free energy per mole of pairs can now be written in the simplified form as

$$2F = + \frac{N\,U_{AA}}{2}\,[X_A{}^2 S_A{}^2(1+3\alpha_A \tau_A{}^2)+ YX_P{}^2 S_P{}^2(1+3\alpha_P \tau_P{}^2)+ 2P\sqrt{Y}\,X_A\,X_P\,S_A\,S_P(1+3\alpha_E \tau_A\,\tau_P\,)]$$

$$- Nk_BTX_A \ln\left(\frac{Z_{Ao}\,Z_{At}}{X_A}\right) - Nk_BTX_P \ln\left(\frac{Z_{Po}\,Z_{Pt}}{X_P}\right) - NX_P\,\Delta E \quad (3.54)$$

The equilibrium value of mole fraction X_A of the A-type of pairs is found by minimising F with respect to X_A. We get (with $X_P = 1 - X_A$)

$$\frac{X_P}{X_A} = \frac{Z_{Po}\,Z_{Pt}}{Z_{Ao}\,Z_{At}} \exp\left\{\frac{U_{AA}}{k_BT}\,[\alpha_A X_A S_A{}^2 \tau_A{}^2 - Y\alpha_P X_P S_P{}^2 \tau_P{}^2 + P\sqrt{Y}\alpha_E S_A S_P \tau_A \tau_P (X_P - X_A)] + \frac{\Delta E}{k_BT}\right\} \quad (3.55)$$

3.4.1.3 Specific heat at constant volume

The molar specific heat at constant volume is give by

$$C_V = \left(\frac{\partial U}{\partial T}\right)_V$$

$$= -\frac{NU_{AA}}{2}\left\{\frac{\partial X_A}{\partial T}\,[X_A S_A{}^2\,(1+\alpha_A \tau_A{}^2) - Y\,X_P S_P{}^2\,(1+\alpha_P \tau_P{}^2)+ P\sqrt{Y}\;S_A\;S_P(1+\alpha_E \tau_A\;\tau_P\,)(X_P - X_A)]\right.$$

$$+ \frac{\partial S_A}{\partial T}\,X_A\,[X_A S_A(1+\alpha_A \tau_A{}^2) + P\sqrt{Y}\,X_P S_P(1+\alpha_E \tau_A \tau_P)]$$

$$+ \frac{\partial S_P}{\partial T}\,X_P\,[YX_P\,S_P(1+\alpha_P \tau_P{}^2)+P\sqrt{Y}\;X_A S_A(1+\alpha_E \tau_A\;\tau_P\,)]$$

$$+ \frac{\partial \tau_A}{\partial T}\,X_A S_A(\alpha_A\,X_A S_A \tau_A + P\sqrt{Y}\,\alpha_E\,X_P\,S_P\,\tau_P)$$

$$\left. + \frac{\partial \tau_P}{\partial T}\,X_P\,S_P(Y\alpha_P\,X_P\,S_P\,\tau_P + P\sqrt{Y}\,\alpha_E\,X_A S_A\,\tau_A)\right\}$$

$$+ \frac{\partial X_A}{\partial T}\,N\Delta E. \quad (3.56)$$

Note that in the above expression, as explained earlier (see section 3.3.1.3), we have not differentiated ΔE with respect to T. Expressions for the derivatives of X_A,

S_A, S_P, τ_A and τ_P and are obtained by differentiating the relevant parameters in the equations 3.52, 3.53 and 3.55 respectively, with respect to T. The five equations obtained after differentiation can be written in the matrix notation as,

$$\begin{bmatrix} C_{11} & C_{12} & C_{13} & C_{14} & C_{15} \\ C_{21} & C_{22} & C_{23} & C_{24} & C_{25} \\ C_{31} & C_{32} & C_{33} & C_{34} & C_{35} \\ C_{41} & C_{42} & C_{43} & C_{44} & C_{45} \\ C_{51} & C_{52} & C_{53} & C_{54} & C_{55} \end{bmatrix} \begin{bmatrix} X'_A \\ S'_A \\ S'_p \\ \tau'_A \\ \tau'_P \end{bmatrix} = \begin{bmatrix} D_1 \\ D_2 \\ D_3 \\ D_4 \\ D_5 \end{bmatrix} \tag{3.57}$$

where the primes indicate the differentiation with respect to T. The expressions for the elements of the matrices are given in the appendix. The relevant derivatives are obtained by solving the five simultaneous equations and hence C_V is calculated.

Apart from the trivial solution corresponding to the isotropic phase, we look for the following types of solutions:

1) S_A, $S_P \neq 0$, $\tau_A = \tau_P = 0$ leading to nematic phase which is N_1 if X_A is small and N_d if X_A is large, and,

2) S_A, $S_P \neq 0$, τ_A , $\tau_P \neq 0$ leading to the smectic phase which is SmA_1 if X_A is small and SmA_d if X_A is large.

3.4.2 Results and discussion

3.4.2.1 ΔE and P independent of α_A: Double reentrance and SmA_1-SmA_d transition

We have carried out the calculations, in the first instance, without including the variation of ΔE or P with α_A. A negative deviation from the GM approximation (*i.e.*, Q <1) is necessary to get a first order SmA_1 - SmA_d transition. The phase diagram obtained with R_1 =15, R_2= 0.6, Q = 0.62 with P = Y= 1, is shown in figure 3.20.

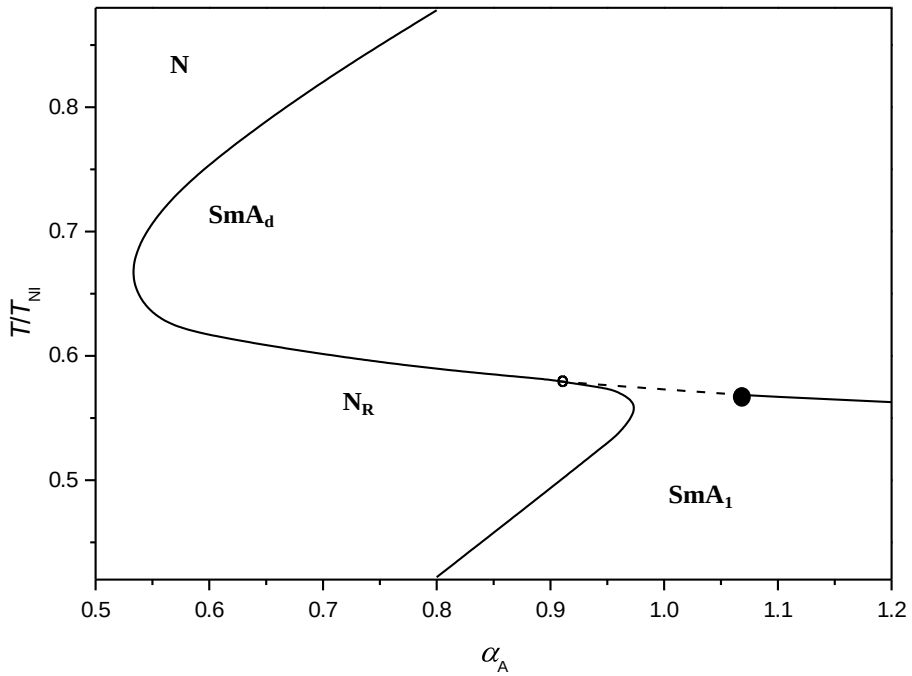

Figure – 3.20. The phase diagram obtained with R_1 =15, R_2= 0.6, Q = 0.62, P = Y= 1 and treating ΔE and P to be independent of α_A. The first order SmA$_1$-SmA$_d$ transition line ends in a critical point (shown by the filled circle). When Q is decreased to 0.55, the SmA$_1$-SmA$_d$ transition line continues (as indicated by the dashed line) and meets the SmA-N$_R$ boundary (shown by the open circle). The remaining parts of the phase diagram do not change perceptibly on decreasing Q.

The first order SmA$_1$-SmA$_d$ transition ends in a critical point at α_A = 1.067 and T_R = 0.56855 (shown by the filled circle). When Q is decreased, the critical point is shifted to lower values of α_A. For Q = 0.55, before ending in a critical point, the SmA$_1$-SmA$_d$ transition line meets the SmA-N$_R$ boundary at α_A = 0.907 and T_R = 0.5796 (shown by the open circle). Note that the critical point is highly sensitive to the value of Q while the other transition temperatures do not change perceptibly on changing the value of Q. This trend is similar to that got in the calculations with saturated nematic order, as already shown in section 3.3.3.1. If we consider P = Q = Y = 1, our model reduces to the model by Madhusudana *et al*, [20], which gives a similar T-α_A phase diagram showing double reentrance, which does not contain a SmA$_1$-SmA$_d$ transition line. In the next subsection, we present the results obtained when the variation of P with α_A is included while ΔE is treated as constant with respect to α_A.

3.4.2.2 Variation of only P with α_A: N - SmA_d - N_{Rd} - N_{R1} - SmA_1 transition sequence

In this subsection, we treat ΔE constant with respect to α_A and include the variation of P with α_A. In this case, for a given set of parameters, the free energy has four local minima with respect to X_A, two corresponding to the nematic phase and two to the smectic phase. Of these, the phase corresponding to the absolute minimum is the stable one. Depending on which two of these four local minima are equal, we get the possibility of various phase transitions.

With Y = 1.4, R_1 = 15, R_2 = 0.6, P^* = 0.15 (recall equation 3.45) and Q = 1, we get the phase diagram shown in figure 3.21. We have already shown, considering a saturated nematic order, that the strong variation of ΔE with α_A (see section 3.3.3.2) leads to an N_R lake associated with the SmA_1-SmA_d transition in the temperature-α phase diagram which corresponds to the experimental temperature-concentration phase diagram. We have also pointed out that this variation is associated with the dissimilarity of the molecules of the two components in the mixture. As mentioned earlier, the strong variation of ΔE with α_A appears to be valid in case of binary mixtures of smectogenic compounds *not* belonging to the same homologous series which show the N_R lake in the temperature-concentration phase diagram. In the mixtures of smectogenic compounds belonging to the *same* homologous series, which show only the SmA_1-SmA_d transition, ΔE can be taken to be practically constant with respect to α_A. As mentioned earlier, α_A is taken to represent the concentration in a mixture. Hence, our results obtained by neglecting the variation of ΔE with α_A can be compared with that obtained by experiments [28] (see figure 3.22a) on a mixture of two compounds DB_8ONO_2 and $DB_{10}ONO_2$ belonging to the *same* homologous series. In the phase diagram, X denotes the mole percentage of the *longer* homologue ($DB_{10}ONO_2$). Obviously, increase of X is equivalent to increase of the McMillan parameter α. For example at X = 53, SmA_d-N_{Rd}-N_{R1}-SmA_1 sequence is seen on cooling. In our calculated phase diagram, for example, at α_A = 0.525, we have N-(0.7)-SmA_d-(0.63)-N_{Rd}-(0.627)-N_{R1}-(0.323)-SmA_1 sequence on cooling, where we have indicated the transition T_R values in parentheses. (For the sake of clarity, the part of the phase diagram below T_R = 0.5 is not shown in the figure 3.21). A reentrant N_d-N_1 transition line which ends at a critical point (at α_A= 0.5123 and T_R =0.6266) is

seen over a small range of α_A (0.5123 to 0.542). As α_A is increased above 0.542, the N_{Rd}-N_{R1} transition line continues as SmA_d - N_{R1} line (for a range of α_A = 0.542 to 0.83) and extends as SmA_d - SmA_1 line (for α_A > 0.83). These features agree with the experimental trends [28], in which there is a reentrant N_d - N_1 transition line which ends at a critical point for lower values of X (see figure 3.22a). As X is increased the N_d - N_1 transition line becomes the SmA_d - N_{R1} transition line and finally continues as SmA_d - SmA_1 transition line.

Keeping R_1, R_2, and Q the same, if Y and P^* are increased to 2 and 0.18 respectively, we get a similar phase diagram shown in the inset of figure 3.21. In this case, the SmA_d-N_{R1} transition occurs over a smaller range of α_A values. These diagrams are also similar to those predicted by the dislocation loop melting theory of Prost and Toner [17] (see figure 3.6 given earlier).

We have evaluated the variation of specific heat at constant volume across the SmA_d-N_{Rd}-N_{R1}-SmA_1 transition sequence at α_A = 0.513 of figure 3.21. The calculated specific heat (figure 3.23) shows a strong peak at the N_{R1}-N_{Rd} transition as seen in the experimental diagram (figure 3.22b). The corresponding variation of the order parameters and X_A are shown in figure 3.24 .

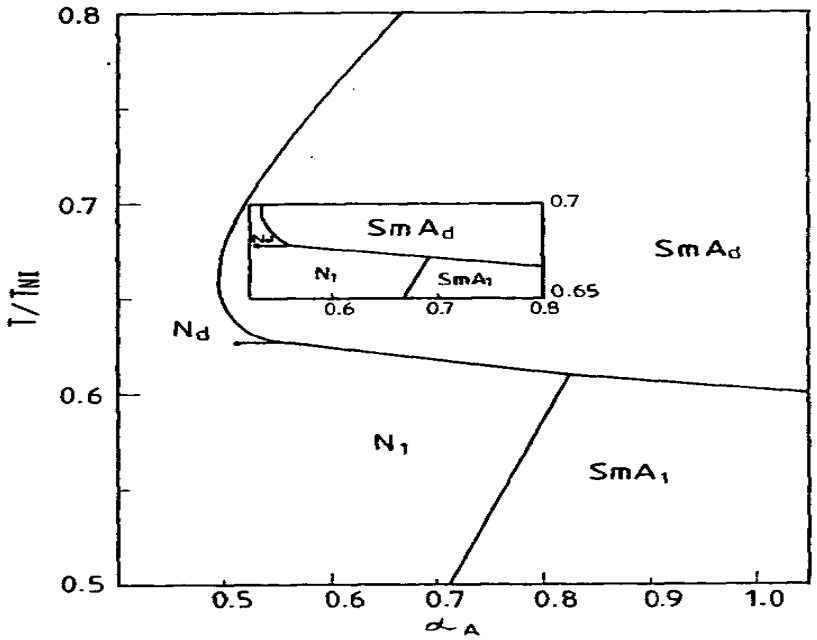

Figure-3.21. Calculated phase diagram with R_1 = 15, R_2 = 0.6, P^* =0.15, Y=1.4 , Q = 1, and treating P to be dependent on α_A, showing the reentrant N_d- N_1 (indicated in the text as N_{Rd} - N_{R1}) transition line starting from a critical point. As α_A is increased the transition line continues as SmA_d -N_1 line and finally as SmA_d - SmA_1 line. The inset is a similar diagram with P^* and Y increased to 0.18 and 2 respectively, showing that SmA_d-N_1 transition occurs over a smaller range of α_A values.

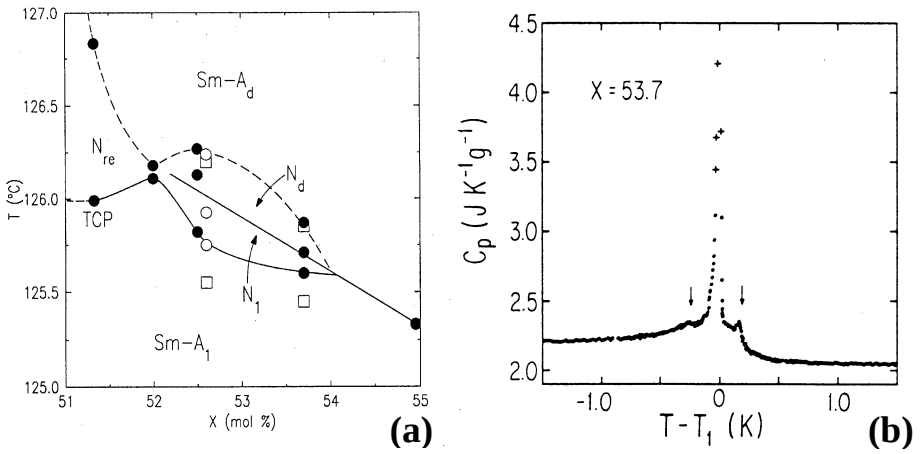

Figure – 3.22. (a) The T-X phase diagram, where X is the mole percent of $DB_{10}ONO_2$ in DB_8ONO_2 [28]. Filled circles, open circles and open squares represent calorimetric, X-ray scattering and optical measurements respectively. The dashed curves indicate 2nd order phase transitions and the solid curves, the 1st order ones. TCP marks the tricritical point. (b)Variation of C_P across the SmA_1-N_1-N_d-SmA_d transition for the mixture with X = 53.7. The strong peak in the middle corresponds to the N_1-N_d transition and the small peak marked by the left arrow corresponds to SmA_1-N_1 and the right arrow to SmA_d-N_d transition.

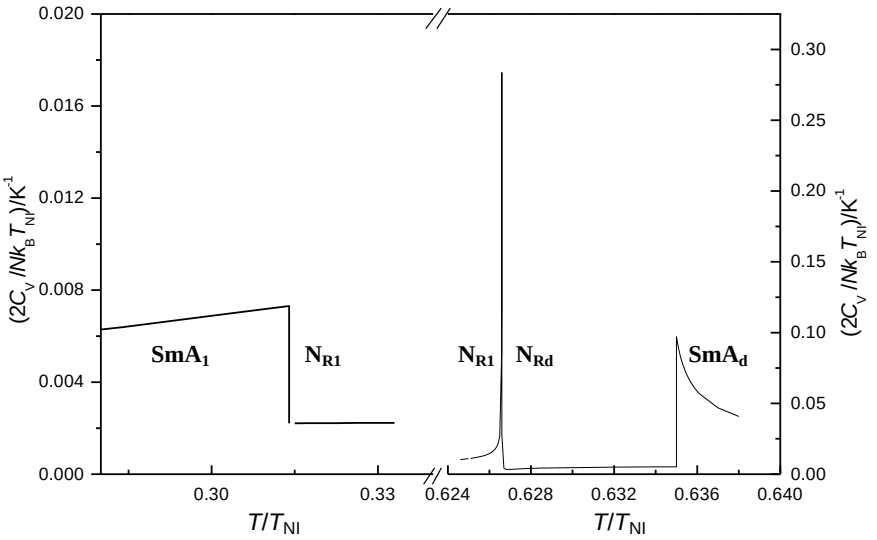

Figure - 3.23. Calculated temperature variation of the specific heat at constant volume (C_v) across the SmA_d-N_{Rd}-N_{R1}-SmA_1 transition at α_A=0.513 as shown in figure 3.21. Note that the scales are different in the left and the right parts of the figure.

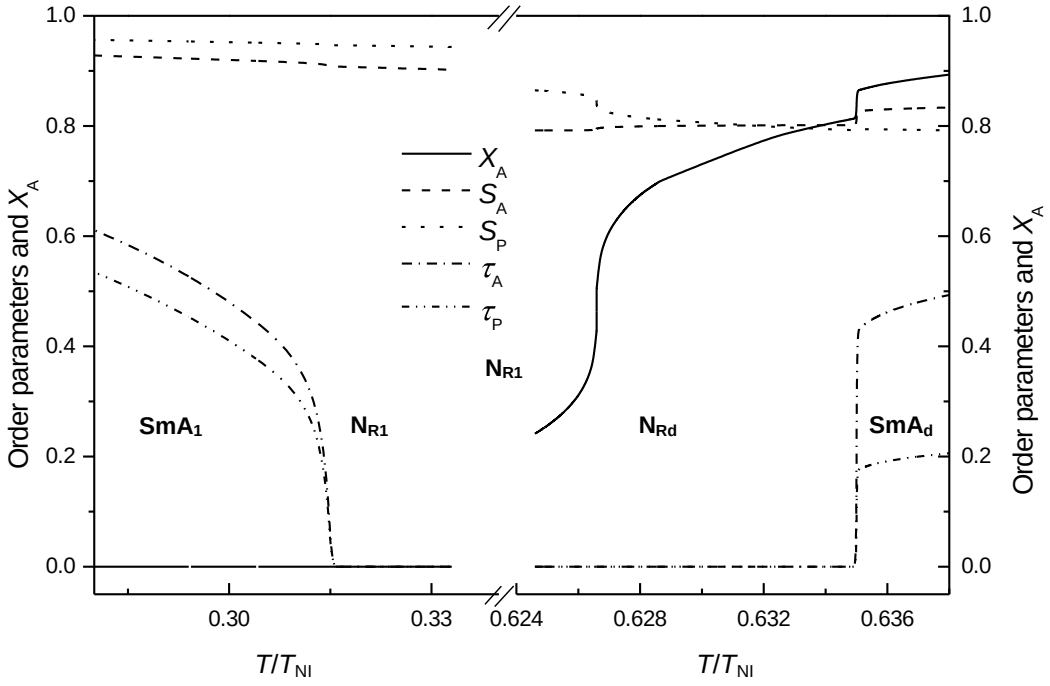

Figure - 3.24. Calculated temperature variations of the order parameters and X_A across the SmA_d - N_{Rd} - N_{R1} - SmA_1 transition at α_A = 0.513 corresponding to figure 3.21. Note that the X-axis scales are different in the left and the right parts of the figure.

The calculated specific heat ($2C_v/Nk_BT_{NI}$) shows a jump ≈ 0.28 for the N_{R1}-N_{Rd} transition. Taking T_{NI} = 500K and the gram molecular weight of DB_9ONO_2 to be ≈ 500 gm, this value corresponds to $\Delta C_v \approx 1$ $JK^{-1}g^{-1}$. This roughly agrees with the experimental value of $\Delta C_P \approx 2$ $JK^{-1}g^{-1}$ (see figure 3.22b). Also, the experimental data indicates that the ΔC_P corresponding to the SmA_1-N_{R1} transition is less than that for the N_{Rd}–SmA_d transition. Our calculations show that the jump in the specific heat at constant volume ΔC_v at the SmA_1-N_{R1} transition is about 10 times less than that at the N_{Rd}-SmA_d transition (see figure 3.23). However, the calculated C_v values can not be expected to have a quantitative agreement with the experimental C_P data. Further, in the SmA_1 and the N_1 phases, the parallel molecules need not be restricted to pairs but can form larger clusters, which has not been taken into account in the theoretical treatment.

In the next subsection we discuss the effect of inclusion of the variation of ΔE with α_A while P is treated as constant with respect to α_A.

3.4.2.3 Variation of only ΔE with α_A: Reentrant nematic lake

We now include the variation of only ΔE with α_A (*i.e.*, $\Delta E \propto \alpha_A^4$, see equation 3.21) and, for the sake of simplicity, ignore the variation of P and Q with respect to α_A. As already discussed, the results of this calculation are to be compared with those of experiments on mixtures of chemically dissimilar compounds. With R_1^*= 6, R_2 =0.7, P= Q =Y = 1, the N_R lake obtained in the T_R-α_A plane is shown in figure 3.25. In our earlier calculations with saturated nematic (section 3.3.3.3) order, we have already shown that the variation of ΔE with α_A leads to an N_R lake. The shape of the N_R lake boundary was elliptical, whereas experimentally it is not found to be so (see figure 3.4c). The shape of the N_R lake boundary obtained in the present calculations is also not elliptical, being wider in the lower α_A side.

As explained in section 3.3.3.3, in this case also, an increase of R_1^* or R_2 leads to a wider lake as shown in figure 3.26 (for R_1^* = 7, R_2 = 0.7) which finally merges with the main nematic sea (for R_1^* = 6, R_2 = 0.75). Also, we have made several calculations including the variation of both ΔE and P with α_A. It not possible in the

present theory to get N_{R1}-N_{Rd} and SmA_1-SmA_d transitions associated with an N_R lake *merging* with the main nematic sea, as it is found in the experiment.

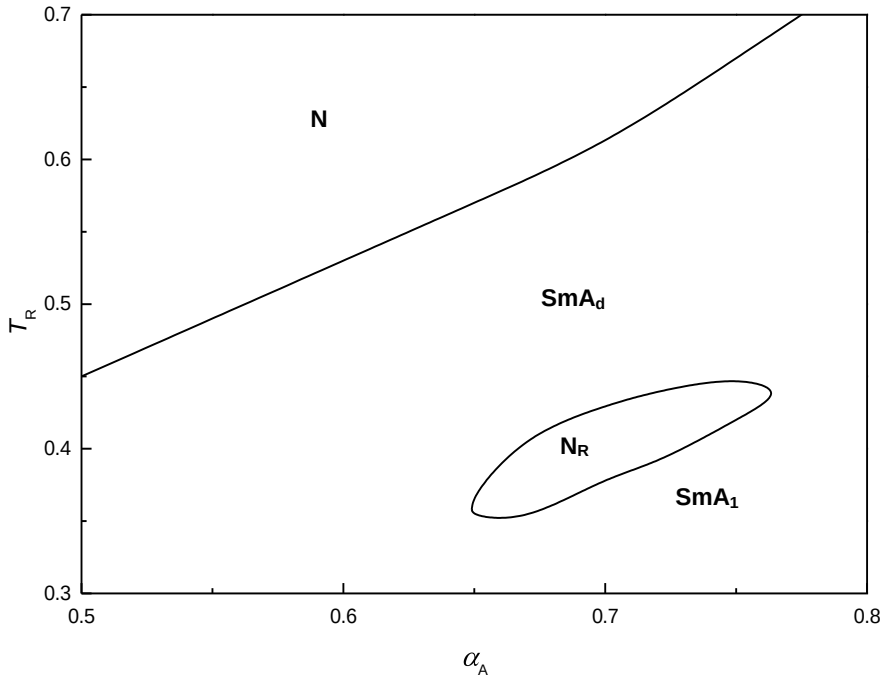

Figure - 3.25. The phase diagram calculated including the variation of

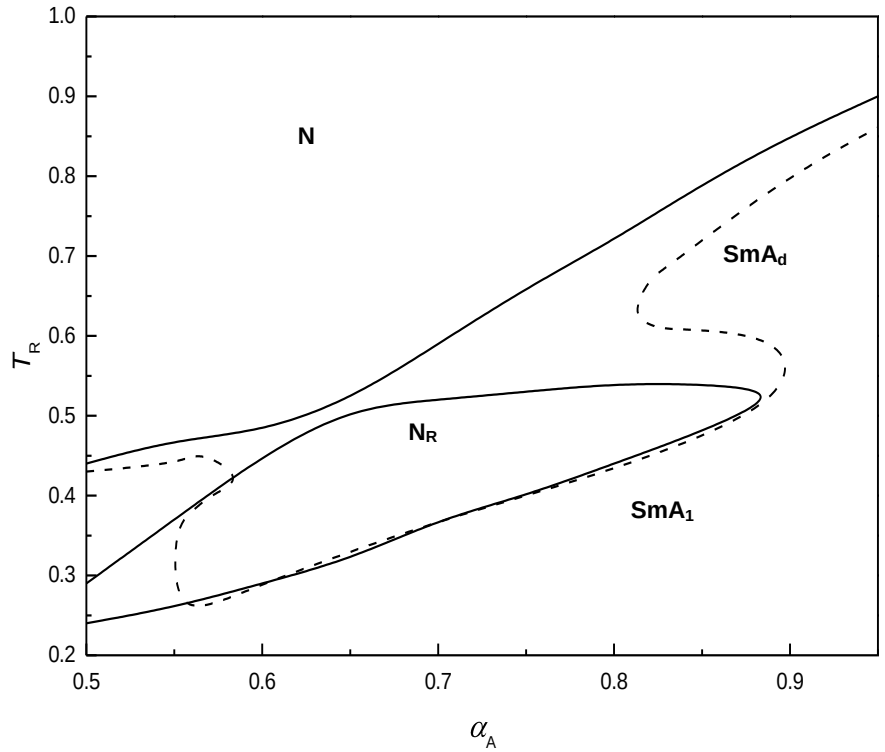

only ΔE with α_A, showing the N_R lake with R_1^* =6, R_2 =0.7 and P=Q=Y=1.

Figure – 3.26. The phase diagram calculated including the variation of only ΔE with α_A, showing the widening and merging of the N_R lake with the nematic sea ($P = Q = Y = 1$). The solid curve is for $R_1^* = 7$, $R_2 = 0.7$ and the dashed one is for $R_1^* = 6$, $R_2 = 0.75$.

While the topology of the calculated phase diagram agrees with the experimental one, the theory overestimates the temperature range of N_R. However, it is to be noted that experiments are done on a mixture of two components belonging to *different* chemical species. Our molecular theory is necessarily over simplified, and a quantitative comparison can not be made. A more detailed theory of *mixtures* of polar compounds might give results which are in closer agreement with the experimental data. We develop a hybrid model in chapter-5, including the hard rod features of the interactions and show that the resulting phase diagrams compare better with the experimental ones.

3.5 Conclusions

In this chapter, we treat the N and SmA liquid crystals made of highly polar molecules to consist of mixtures of parallel and antiparallel molecular pairs to develop a simple molecular mean field theory. We have argued that the configurational energy difference between the two types of pairs as well as the negative deviation from the GM rule for the mutual attractive interaction between them vary with the McMillan parameter α_A. We first treat the nematic order to be saturated and calculate various phase diagrams as functions of model parameters. Our theory explains the phenomenon of double re-entrance, first order smectic A_1 to smectic A_d transition ending at a critical point and the appearance of a re-entrant nematic lake associated with the SmA_1-SmA_d transition [30]. Next, we have extended the theory [31] to include the orientational interactions and an appropriate deviation from the GM rule. It is shown that as the McMillan parameter α_A (and hence the chain length in a homologous series) is decreased, SmA_d - SmA_1 line goes over to the SmA_d-N_{R1} line which finally becomes the N_{Rd}-N_{R1} transition line, the latter ending in a critical point, as seen experimentally. Also, for a range of values of α_A, we get the possibility of N-SmA_d-N_{Rd}-N_{R1}-SmA_1 phase sequence on cooling. The N_{Rd}- N_{R1} transition occurs over a very small range of α_A. The shape of the boundary of the N_R lake obtained after the

inclusion of the nematic interactions is in better agreement with the experimental results compared to that obtained with a saturated nematic order.

3.6 Appendix

Elements of the matrix (see equation 3.57) used to calculate the derivatives are as follows:

C_{i1} are the coefficients of $\frac{\partial X_A}{\partial T}$,

$$C_{11} = \frac{U_{AA}}{k_B T}\left[2P\sqrt{Y}\ S_A S_P(1+\alpha_E \tau_A \tau_P) - S_A{}^2 (1+\alpha_A \tau_A{}^2) - Y S_P{}^2 (1+\alpha_P \tau_P{}^2)\right] + \frac{1}{X_A X_P}$$

$$C_{21} = \frac{U_{AA}}{k_B T}\left[S_A(1+\alpha_A \tau_A{}^2) - P\sqrt{Y}\ S_P (1+\alpha_E \tau_A \tau_P)\right]$$

$$C_{31} = \frac{U_{AA}}{k_B T}\left[P\sqrt{Y}\ S_A (1+\alpha_E \tau_A \tau_P) - Y S_P (1+\alpha_P \tau_P{}^2)\right]$$

$$C_{41} = \frac{U_{AA}}{k_B T} S_A(\alpha_A S_A \tau_A - P\sqrt{Y}\ \alpha_E S_P \tau_P)$$

$$C_{51} = \frac{U_{AA}}{k_B T} S_P(P\sqrt{Y}\ \alpha_E S_A \tau_A - Y\alpha_P S_P \tau_P)$$

C_{i2} are the coefficients of $\frac{\partial S_A}{\partial T}$,

$$C_{12} = \frac{U_{AA}}{k_B T}\left[P\sqrt{Y}\ X_A S_P(1+\alpha_E \tau_A \tau_P) - X_A S_A(1+\alpha_A \tau_A{}^2)\right]$$

$$C_{22} = \frac{U_{AA}}{k_B T}\left[X_A(1+\alpha_A \tau_A{}^2)\right] - \frac{1}{\Delta A}$$

$$C_{32} = \frac{U_{AA}}{k_B T}\left[P\sqrt{Y}\ X_A(1+\alpha_E \tau_A \tau_P)\right]$$

$$C_{42} = \frac{U_{AA}}{k_B T}\left[2\alpha_A X_A S_A \tau_A + P\sqrt{Y}\ \alpha_E X_P S_P \tau_P\right]$$

$$C_{52} = \frac{U_{AA}}{k_B T}\left[P\sqrt{Y}\ \alpha_E X_A \tau_A S_P\right]$$

Where we have used $\Delta A = \langle [P_2\cos(\theta_i)_A]^2 \rangle - S_A^2$

C_{i3} are the coefficients of $\frac{\partial S_P}{\partial T}$,

$$C_{13} = \frac{U_{AA}}{k_B T}[YX_P S_P(1+\alpha_P \tau_P^2) - P\sqrt{Y}\, X_P S_A(1+\alpha_E \tau_A \tau_P)]$$

$$C_{23} = \frac{U_{AA}}{k_B T}[\, P\sqrt{Y}\, X_P(1+\alpha_E \tau_A \tau_P)]$$

$$C_{33} = \frac{U_{AA}}{k_B T}[\, YX_P(1+\alpha_P \tau_P^2)] - \frac{1}{\Delta P}$$

$$C_{43} = \frac{U_{AA}}{k_B T}[\, P\sqrt{Y}\, \alpha_E X_P \tau_P S_A]$$

$$C_{53} = \frac{U_{AA}}{k_B T}[2Y\alpha_P X_P S_P \tau_P + P\sqrt{Y}\, \alpha_E X_A S_A \tau_A]$$

Where we have used $\Delta P = \langle [P_2\cos(\theta_i)_P]^2 \rangle - S_P^2$

C_{i4} are the coefficients of $\frac{\partial \tau_A}{\partial T}$,

$$C_{14} = \frac{U_{AA}}{k_B T}\,[S_A(P\sqrt{Y}\, \alpha_E X_A S_P \tau_P - \alpha_A \tau_A X_A S_A)]$$

$$C_{24} = \frac{U_{AA}}{k_B T}\,[P\sqrt{Y}\, \alpha_E X_P S_P \tau_P + 2X_A S_A \alpha_A \tau_A]$$

$$C_{34} = \frac{U_{AA}}{k_B T}\,[P\sqrt{Y}\, \alpha_E X_A S_A \tau_P]$$

$$C_{44} = \frac{U_{AA}}{k_B T}\,[\alpha_A X_A S_A^2] - \frac{1}{\Delta AS}$$

$$C_{54} = \frac{U_{AA}}{k_B T}\,[P\sqrt{Y}\, \alpha_E X_A S_A S_P]$$

Where we have used $\Delta AS = \langle [\cos(2\pi z_{Ai}/d)]^2 \rangle - \tau_A^2$

C_{i5} are the coefficients of and

$$C_{15} = \frac{U_{AA}}{k_B T}\,[S_P(Y\alpha_P \tau_P X_P S_P - P\sqrt{Y}\, \alpha_E X_P S_A \tau_A)]$$

$$C_{25} = \frac{U_{AA}}{k_B T} [P\sqrt{Y}\, \alpha_E X_P S_P \tau_A]$$

$$C_{35} = \frac{U_{AA}}{k_B T} [P\sqrt{Y}\, \alpha_E X_A S_A \tau_A + 2Y\alpha_P X_P S_P \tau_P]$$

$$C_{45} = \frac{U_{AA}}{k_B T} [P\sqrt{Y}\, \alpha_E X_P S_P S_A]$$

$$C_{55} = \frac{U_{AA}}{k_B T} [Y\alpha_P X_P S_P{}^2] - \frac{1}{\Delta BS}$$

Where we have used $\Delta BS = \langle [\cos(2\pi z_{Pi}/d)]^2 \rangle - \tau_p{}^2$

D_i are the terms not connected with the derivatives.

$$D_1 = \frac{U_{AA}}{k_B T^2} [YX_P S_P{}^2(1+\alpha_P \tau_P{}^2) - X_A S_A{}^2(1+\alpha_A \tau_A{}^2) - P\sqrt{Y}\, S_A S_P(1+\alpha_E \tau_A \tau_P)(X_P - X_A)] + \frac{\Delta E}{k_B T^2}$$

$$D_2 = \frac{U_{AA}}{k_B T^2} [X_A S_A(1+\alpha_A \tau_A{}^2) + P\sqrt{Y}\, X_P S_P(1+\alpha_E \tau_A \tau_P)]$$

$$D_3 = \frac{U_{AA}}{k_B T^2} [YX_P\, S_P(1+\alpha_P \tau_P{}^2) + P\sqrt{Y}\; X_A S_A(1+\alpha_E \tau_A\, \tau_P)]$$

$$D_4 = \frac{U_{AA}}{k_B T^2} [S_A(\alpha_A\, X_A S_A \tau_A + P\sqrt{Y}\, \alpha_E\, X_P\, S_P \tau_P)]$$

$$D_5 = \frac{U_{AA}}{k_B T^2} [S_P(Y\alpha_P\, X_P\, S_P \tau_P + P\sqrt{Y}\, \alpha_E\, X_A S_A \tau_A)]$$

3.7 References for chapter-3

[1] Gray, G. W, in *Advances in Liquid Crystals*, vol.2, (ed. G. H. Brown, Academic Press, New York, 1976), p32.

[2] Cladis, P. E., *Phys. Rev. Lett*., **35**, 48,1975.

[3] Cladis, P. E., Bogardus, R. K., Daniels, W. B., and Taylor, G. N.,*Phys. Rev. Lett*., **39**, 720, 1977.

[4] Hardouin, F., Sigaud, G., Achard, M. F and Gasparoux, H, *Phys.lett*, A**71**, 347, 1979; Madhusudana, N. V., Sadashiva, B. K., and Moodithaya, K. P. L, *Curr. Sci.*, **48**, 613, 1979.

[5]Guillon, D., Cladis, P. E., and Stamatoff, J.,*Phys. Rev. Lett*, **41**,1598,1978.

[6]Hardouin, F., Levelut, A. M., Achard, M. F. and Sigaud, G., *J.chim.phy*, **80**, 53, 1983.

[7]Cladis, P. E., in *Liquid Crystals*, ed Chandrashekhar, S., Heyden Publ, Philadelphia,1980, p105.

[8] Hardouin, F., Sigaud, G., Achard, M. F and Gasparoux, H, *sol. st. commun.*, **30**, 265, 1979.

[9] Tinh, N. H., Hardouin, F., and Destrade, C., *J. Physique*, **43**, 1127, 1982.

[10]Shashidhar, R., Ratna, B. R., Surendranath, V., Raja, V. N., Krishna Prasad, S. and Nagabhushan, C., *J.phys.lett.*, **46**, L-445, 1985.

[11] Raja, V. N., Ratna, B .R., Shashidhar, R., Heppke, G., Bahr., Ch, Marko, J. F., Indeku, J. O., Berker. A. N., *Phys. Rev A*, **39**, 4341, 1989.

[12]Pfieffer, S., Heppke, G., Shankar Rao, D. S. and Shashidhar, R., *Phys. Rev A*, **46**, 6166, 1992.

[13]Brodzik, M. and Dabrowski, R., *Liq. Cryst*, **18**, 61, 1995.

[14]Shashidhar, R., and Ratna, B. R., *Liq. Cryst.*, **5**, 421, 1989.

[15]Shashidhar, R., Ratna, B. R., Krishna Prasad, S., and Somasekhara, S., *Phys. Rev. Lett*, **59**, 1209, 1987.

[16]deGennes, P. G., and Prost, J., *The Physics of liquid crystals*, 2nd edition, Clarendon press, Oxford, 1993.

[17]Prost, J., and Toner, J., *Phy. Rev. A*, **36**, 5008,1987.

[18]Madhusudana . N . V and Chandrasekhar. S. Pramana Suppl., **1**,57, 1973.

[19]Hardouin, F. and Levelut, A. M., *J. Phys*, **41**, 41, 1980.

[20]Madhusudana, N. V., and Jyothsna Rajan, *Liq.Cryst.*, **7**, 31, 1990.

[21] Basappa, G., and Madhusudana, N.V., *Eur. Phys. Journal B*, **1**, 179, 1998.

[22]McMillan, W. L., *Phy. Rev. A*, **4**, 1238, 1971.

[23] Maier, W., and Saupe, A., *Z.Naturforsch*, **A14**, 882, 1959.

[24]Czuprynski, K., Dabrowski, R., Baran, J., Zywocinski, A., Przedmojski, J., *J.*Phys, **47**, 1577, 1986.

[25]Hardouin, F., Achard, M.F., Tinh, N.H., and Sigaud, G., *Mol. Cryst. Liq. Cryst. Lett.*, **3**, 7, 1986.

[26]Marko, J.F., Indekeu, J.O., and Nihat Berker, A., *Phy.Rev.* **39A**, 4201,1989.

[27]Wu Lei, Garland, C.W., and Pfeiffer, S., *Phys.Rev.A*, **46**, 973, 1992.

[28]Nounesis, G., Kumar, S., Pfeiffer, S., Shashidhar, R., and Garland,C.W., *Phy. Rev. Lett*, **73** , 565, 1994.

[29]Katriel J. and Kventsel G. F., *Phys.Rev.A*, **28**, 3037,1983.

[30]Govind, A. S., and Madhusudana, N. V., *Liq. Cryst.*, **23**, 327, 1997.

[31]Govind, A. S., and Madhusudana, N. V., *Liq. Cryst.*, **27**, 215, 2000.